frontiers | Frontiers in Earth Science

ORIGINAL RESEARCH
published: 07 July 2022
doi: 10.3389/feart.2022.894582

Ultramafic Rocks and Their Alteration Products From Northwestern Allaqi Province, Southeastern Desert, Egypt: Petrology, Mineralogy, and Geochemistry

A. M. Abdel-Rahman[1], H. M. El-Desoky[1], B. N. A. Shalaby[2], H. A. Awad[3], Antoaneta Ene[4], M. A. Heikal[1], H. El-Awny[1], W. Fahmy[1], S. A. Taalab[1] and Hesham M. H. Zakaly[5,6†]**

[1]Geology Department, Faculty of Science, Al-Azhar University, Cairo, Egypt, [2]Geology Department, National Research Center, Cairo, Egypt, [3]Geology Department, Faculty of Science, Al-Azhar University, Assuit, Egypt, [4]INPOLDE Research Center, Department of Chemistry and Physics and Environment, Faculty of Sciences and Environment, Dunarea de Jos University of Galati, Galati, Romania, [5]Institute of Physics and Technology, Ural Federal University, Yekaterinburg, Russia, [6]Physics Department, Faculty of Science, Al-Azhar University, Cairo, Egypt

The ophiolitic rocks, island arc metasediments, and granitic rocks are encountered in the study of the Allaqi province. The present study concentrated on ultramafic rocks and their various forms of hydrothermal alteration. Ophiolites commonly occur as dismembered rock sequences and have different types of hydrothermal alteration products. Ophiolites contain the essential type as serpentinites and talc-carbonate rocks, listwaenites, and amphibolites along shear zones and faults. Listwaenite is one of the most significant rocks in this area because it contains gold. The whole serpentinite rocks are affected by regional metamorphosis into greenschist facies. Geochemically, Neoproterozoic serpentinites fall into SSZ ophiolites, alpine-type peridotite, formed in the forearc peridotite tectonic environment. Regardless, the listwaenite and talc-carbonate rocks revealed that they trend to silica, carbonate, and talc. Listwaenites are classified into two types: carbonate-rich listwaenites and silica–carbonate-rich listwaenites. Magnetite, chromite, galena, and gold are the most typical ores recorded in this research.

Keywords: ophiolite, ultramafic rocks, serpentinization, listwaenite, carbonization, REE

OPEN ACCESS

Edited by:
Zhilei Sun,
Qingdao Institute of Marine Geology (QIMG), China

Reviewed by:
Mokhles Azer,
National Research Centre, Egypt
Weiliang Liu,
Sun Yat-sen University, China
Petros Koutsovitis,
University of Patra, Greece

****Correspondence:***
Antoaneta Ene
Antoaneta.Ene@ugal.ro,
Hesham M. H. Zakaly
h.m.zakaly@gmail.com
h.m.zakaly@azhar.edu.eg

†ORCID:
Hesham M. H. Zakaly
orcid.org/0000-0002-7645-9964

Specialty section:
This article was submitted to Geochemistry, a section of the journal Frontiers in Earth Science

Received: *11 March 2022*
Accepted: *13 May 2022*
Published: *07 July 2022*

Citation:
Abdel-Rahman AM, El-Desoky HM, Shalaby BNA, Awad HA, Ene A, Heikal MA, El-Awny H, Fahmy W, Taalab SA and Zakaly HMH (2022) Ultramafic Rocks and Their Alteration Products From Northwestern Allaqi Province, Southeastern Desert, Egypt: Petrology, Mineralogy, and Geochemistry. Front. Earth Sci. 10:894582. doi: 10.3389/feart.2022.894582

1 INTRODUCTION

Neoproterozoic ophiolites are prosperous in the Arabian–Nubian Shield (ANS) and vary in age from 690 to 890 million years ago and up to 100 Ma (from 780 to 680 Ma) of terrane development in suture zones (Stern, 1994; Loizenbauer et al., 2001; Stern et al., 2004; Ali et al., 2010). Mafic-ultramafic rocks constitute one of the distinctive rock units in the Egyptian basement. The Egyptian Neoproterozoic mafic/ultramafic comprises about 5% of all Precambrian outcrops in the Eastern Desert of Egypt (Dixon, 1979). Understanding the tectonic settings of the modern and ancient ocean crust (e.g., ophiolite sequences) in the ANS is crucial to understanding the Pan-African orogeny's development (Dilek and Newcomb, 2003). Mid-ocean ridge basalt (MORB) ophiolites and supra-subduction zone (SSZ) ophiolites are the two common types of ophiolite sequences (Pearce et al., 1984; Dilek et al., 2008). MORB ophiolites are classified as E-MORB, P-MORB, N-MORB, and C (contaminated)-MORB categories (Pearce, 2008).

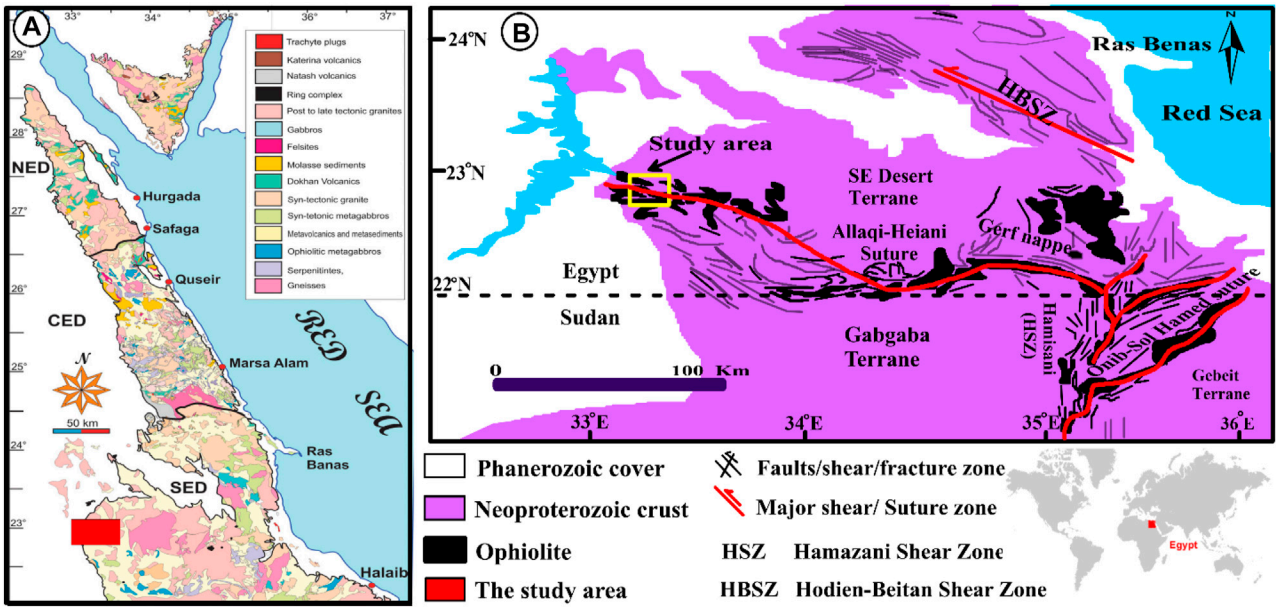

FIGURE 1 | (A) Geological map of the Egyptian Nubian Shield compiled after the geological map of Egypt (El-Ramly, 1972) and the CONCO geological maps (Klitzch et al., 1987). **(B)** Location of the study area with structural features in the southern part of the Egyptian Shield, compiled from Sultan et al. (1987) and Greiling et al. (1994). Abbreviation: NED: North Eastern Desert, CED: Central Eastern Desert, and SED: South Eastern Desert.

The northern part of the Nubian Shield is exhibited by the Precambrian rocks of the Eastern Desert of Egypt. The Central (CED) and Southeastern (SED) deserts of Egypt are abundant in Neoproterozoic dismembered ophiolite assemblages (**Figure 1A**; Shackleton et al., 1980; Ries et al., 1983; El-Desoky and Khalil, 2011; El-Desoky et al., 2015; Abdel-Karim et al., 2016; Zakaly et al., 2019, El-Bahariya, 2019; Awad et al., 2021, El-Bahariya, 2021 and Awad et al., 2022a, Awad et al., 2022b). The presence of listwaenites in association with serpentinites denotes that the Egyptian ophiolite is silicified and carbonated along a regional scale stretching about 500 km in many areas of the South and Central Eastern Desert (Oweiss et al., 2001; Kusky and Ramadan, 2002; Botros, 2004; Zoheir and Lehmann, 2011; El-Desoky and Saleh, 2012). Previous studies of ophiolites in the southern part of Egypt are scarce; therefore, this research is a new addition to geological studies in the southern region of Egypt. This article detailed the geology, petrography, tectonic setting, and geochemistry of ophiolitic ultramafic rocks in the studied region and their alteration types and identified the ore minerals hosted in Neoproterozoic serpentinite and listwaenite in the northwesternmost Allaqi–Heiani suture, Southeastern Desert of Egypt. These results are useful for determining the significance and evolution of these rocks in the ANS, as well as their link to mineralization.

2 GEOLOGICAL BACKGROUND

The Allaqi–Heiani–Gerf and Onib–Sol Hamed suture zones include the majority of the ophiolitic sequences in the Southeastern Desert (**Figure 1B**). From Lake Nasser to the Red Sea, the huge portion may be tracked through the Allaqi–Heiani suture, Gerf nappe, and Sol Hamid ophiolite for a distance of nearly 400 km.

The Allaqi suture separates the Gerf terranes (also known as the Aswan, Midyan) and Southeastern Desert of Egypt terranes (Kroner et al., 1987; Greiling et al., 1994; Shackleton, 1994; Abdelsalam and Stern, 1996), on the north from the 830–720 Ma Gabgaba terranes also known as the Hijaz-Gebeit terranes on the south (Abdelsalam and Stern, 1996). As it joins with and is overprinted by the NNE-trending Hamizana shear zone, the suture strikes nearly east but swings to the southeast (HSZ; **Figure 1B**). The Allaqi suture area includes gneiss, dismember ophiolites, island arc volcano-sedimentary assemblages, and syn- to post-orogenic rocks (e.g., Kroner et al., 1987; Abd El-Naby and Frisch 2002; Abdelsalam et al., 2003; Zoheir and Klemm 2007; Ali et al., 2010). Mafic and ultramafic rocks, as well as their alteration products, comprise the nappes that make up fragmented ophiolite assemblages. The serpentinites represent a distinctive lithology of dismembered ophiolites of the western YOSHGAH suture. Some areas include primary mineral relics, while others have been severely changed, notably along with thrusts and shear zones, with the formation of talc, talc-carbonate, and reddish-brown quartz-carbonate rocks (listwaenite mineral deposits such as gold, chromite, magnesite, and talc can be hosted in this suture (Klemm et al., 2001; Oweiss et al., 2001; Kusky and Ramadan 2002; Azer 2013). Several isolated serpentinized peridotite masses occur in the north half of the Wadi Allaqi district, the study area, and have been regarded as relics of ophiolites in regional geologic maps of the Southeastern Desert. They are recorded in Gabel Shikeyite, Wadi Haimur, and Umm Arakah (**Figure 2A**). The serpentinized peridotite sheets are bounded by linear thrust fault

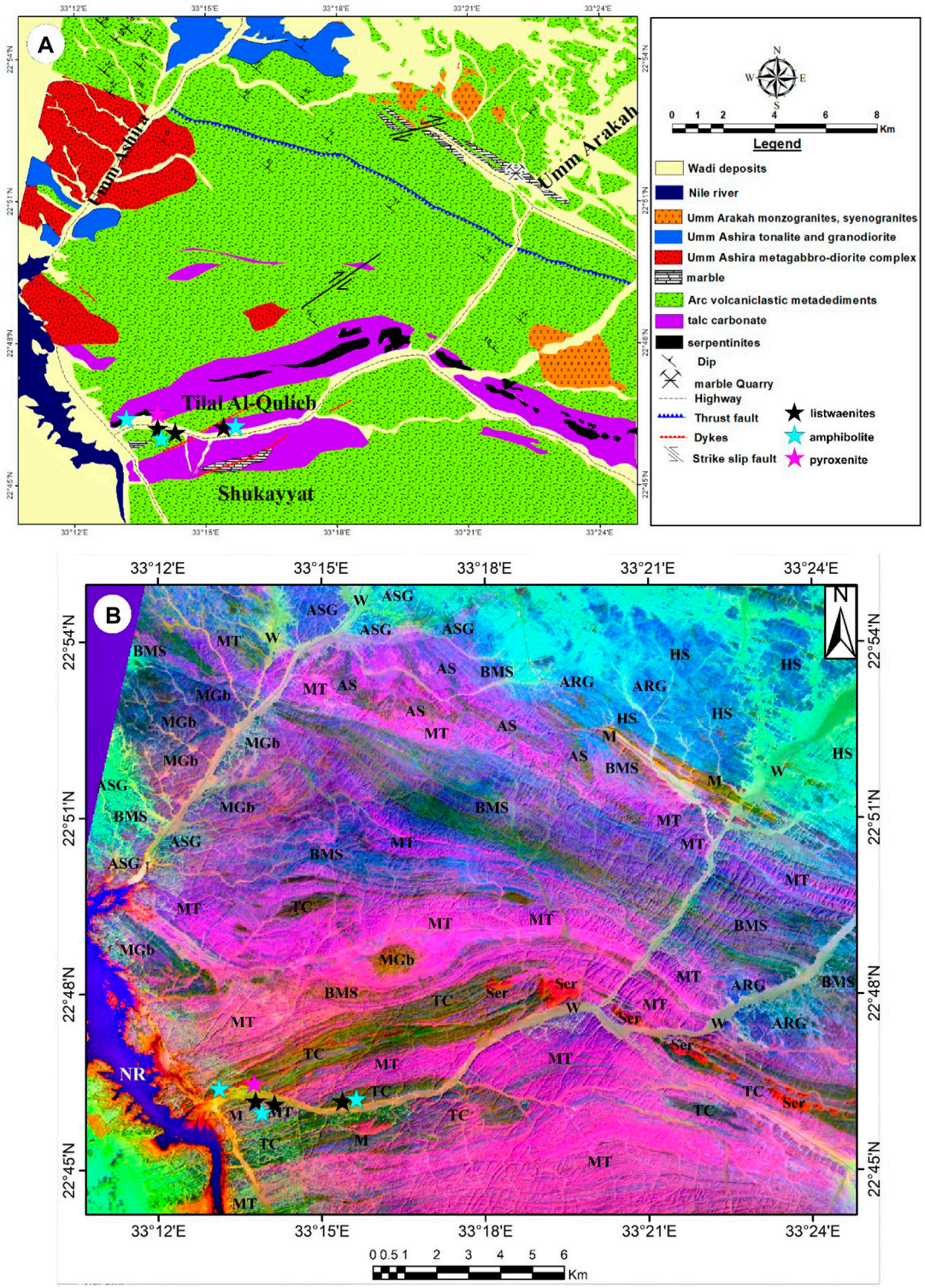

FIGURE 2 | (A) Geologic map of Wadi Tilal Al-Qulieb and Wadi Um Ashira areas modified after Noweir et al. (2000). **(B)** Location map of the studied area according to the PCA (PC3, PC1, and PC4 in RGB) image. Abbreviation: ARG, Umm Arka granites; AS, actinolite schist; ASG, Umm Ashira granite; BMS, biotite and muscovite schist; HS, hornblende schist; M, marble; MGb, metagabbro; MT, metamudstones and metatuffs; NR, Nile River; Ser, serpentinite; TC, talc-carbonate and W, Wadi deposits.

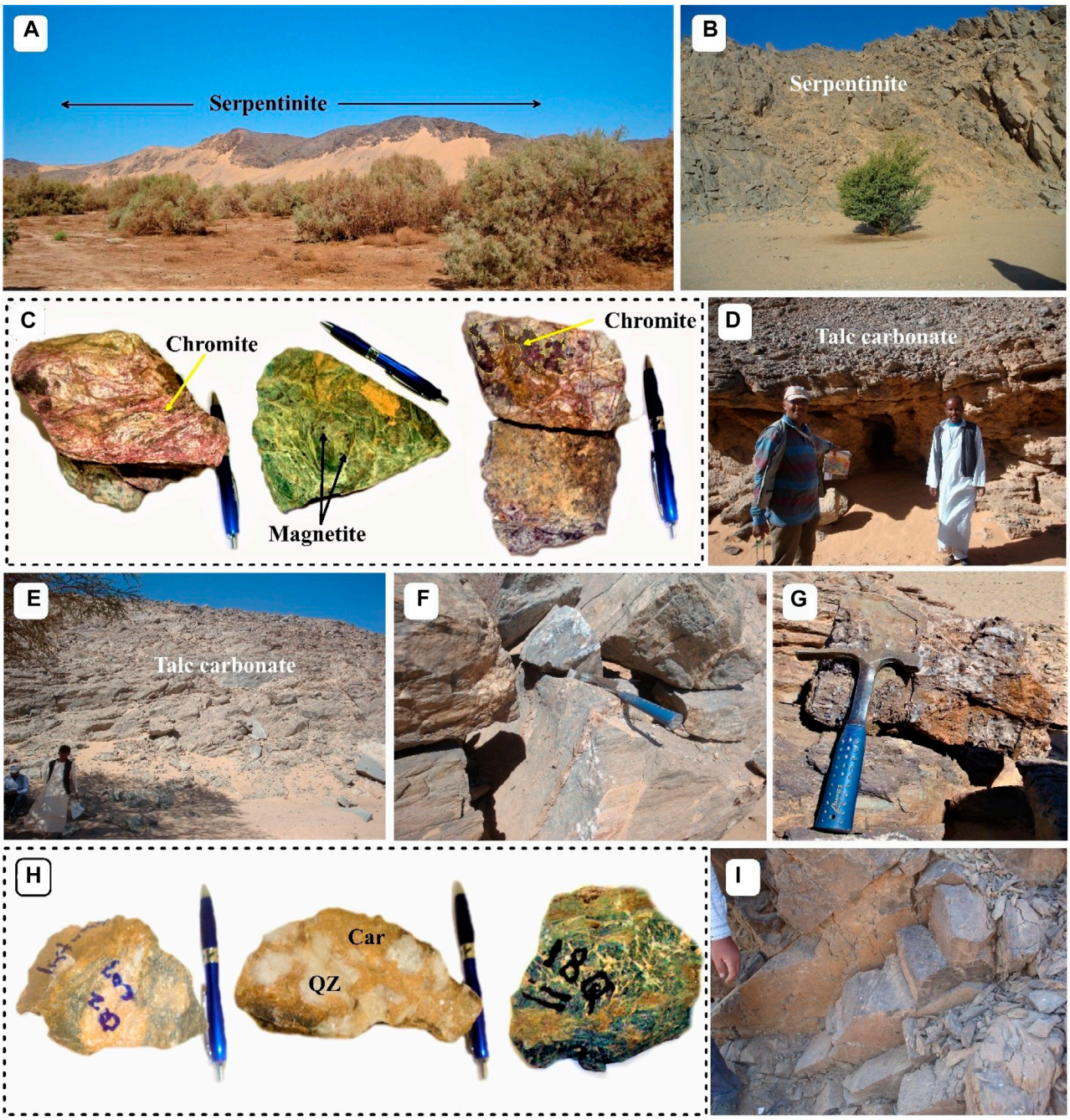

FIGURE 3 | Field photograph showing the studied rocks: **(A,B)** Continuous ridge of serpentinite rocks (Looking N-W). **(C)** Magnetite and chromite bearing serpentinite samples along a shear zone. **(D)** Talc-carbonate rocks exhibiting the conspicuous cavernous structure (Looking N-W). **(E)** Creamy talc carbonates (Looking N-W). **(F)** Massive listwaenite rocks. **(G)** Porous listwaenite. **(H)** Different types of listwaenite rocks. **(I)** Exposed surface of colonnade columnar joints in amphibolites.

planes, indicating that they are tectonically emplaced. The ophiolite is the oldest rock unit in the study region (Akaad and Noweir, 1980), and it defines the Allaqi–Heiani ophiolite belt northern continuation (Kroner et al., 1987). They are overlain by the metavolcavic–metasedimentary succession and intruded by syn-tectonic granitoids. According to the geologic map after Noweir et al. (2000), all the studied rock units are comprising dismember ophiolites derivatives, island arc assemblage, and late to postorogenic intrusions (**Figure 2A**). The study area under consideration constitutes a part of the basement complex of the southeastern desert of Egypt. It is located at the northwestern segment of the Wadi Allaqi terrain, 170 km southeast of Aswan (longitudes 33°15'–33°30'E and latitudes 22°40'–23°00'N; **Figure 2A**).

3 FIELD OBSERVATIONS

The basement complex cropping out around Wadi Tilal Al-Qulieb and Wadi Umm Ashira districts comprise ultramafic ophiolite rocks, arc volcaniclastic metasediments, metagabbro-diorite, and late to post-tectonic stage rocks (**Figure 2A**). A geological map of the entire examined region has been developed based on the principal component analysis approach (PC2, PC1, and PC4 in RGB, respectively), used in this study by ASTER picture (Soliman et al., 2021; **Figure 2A**) and comprehensive field observations (**Figure 2B**). It considers a good image, which shows the lithologic and structural edge of ultramafic rocks (**Figure 2B**).

The ultramafic rocks in the study area can be differentiated into two types based on the degree of deformation and metamorphic processes. The first is a massive serpentinite, which still retains relics of pyroxenites. The second is highly sheared ultramafic rocks transformed into quartz-carbonate (listwaenite) and talc-carbonate rocks. The ophiolitic rocks exposed in the study area include mainly serpentinites, talc-carbonate rocks, listwaenite, and amphibolite, as well as minor outcrops of pyroxenite. Amphibolite, talc carbonate, and listwaenite lenses are also encountered in some unmappable areas. The serpentinites are the oldest rocks and being exposed along the flank of Wadi Tilal Qulieb. They form disrupted allochthonous and discontinuous remnants (**Figure 3A**). Serpentinites are displaying high blocks, lenses, and elongated masses. The lenses and blocks extended in a NW-SE direction and parallel to the regional structural trend of the studied district (Noweir et al., 2000). They are thrusting over the metasediments of wadi Hosarba, showing irregular contact, minor folds, and shearing indicators.

It is massive but sometimes sheared and foliated along the shear zone (**Figure 3B**). These are greenish-black or pale violet to dark purple in color (**Figure 3C**). In some samples, the presence of small black magnetite crystals can be observed near shear zones (**Figure 3C**).

Talc-carbonate rocks are recorded in Wadi Tilal Al-Qulieb, (**Figure 3D, E**). The talc-carbonate rocks are soft and fine-grained with a talcose touch. In some places, biological structures were observed with a clear cavernous structure (**Figure 3D**). It is characterized by creamy to gray in color, and as huge areas dispersed unevenly in serpentinites. Listwaenites have been identified in the southern portions of the Wadi Tilal Al-Qulieb area (North Shukayyat; **Figure 3F**). The oxidation of Fe-bearing carbonates is responsible for the reddish-brown surface appearance. Listwaenite generally has a well-developed porous texture (**Figure 3G**). These massive rocks are relatively resistant to weathering if compared with the surrounding rocks; accordingly, and it stands out forming prominent topographic ridges. Listwaenite is distinguished by several colors ranging from white to reddish-brown and porous texture (**Figure 3H**). Pyroxenites are found in ultramafic rocks as unmappable pockets, lenses, or shear pods. These rocks appear as masses of fine-to medium-grained crystals in a dark gray to black color. Amphibolites are fine-to medium-grained and unmappable also, ranging from greenish gray to black. It is defined by columnar-jointed colonnades (**Figure 3I**). Amphibolites are exposed to the southeast of Wadi Tilal Al-Qulieb and the northern part of the Shukayyat area. Typically, they are medium- to coarse-grained and composed of hornblende and plagioclase. These are the diagnostic rocks of the amphibolite facies of regional metamorphism and may be derived from pre-metamorphic rocks of various types.

4 ANALYTICAL TECHNIQUES

A total of roughly 30 fresh samples from the Tilal Al-Qulieb complex's ultramafic rocks were gathered. Polarizing and ore microscopy inspections were used to prepare all samples for thin section and thin-polished examinations. These methods reveal the mineral composition, textures, microstructures, and alteration types of the investigated rocks, as well as identify opaque minerals and their intergrowth and replacement textures.

Representative chemical analysis of 13 rock samples revealed the presence of major, trace, and rare earth elements. Major oxides, trace, and rare earth elements were analyzed using inductively coupled plasma (ICP) techniques. Samples were tested as powder bullets, and 1 gram was used to determine moisture content by burning to 110°C, followed by 900°C to determine loss on ignite (LOI). Following a lithium metaborate/tetrabortate fusion and dilute nitric digestion, a 0.2 g sample was examined by ICP-emission spectrometry for trace and rare earth elements. In addition, a duplicate 0.5 g split is digested in aqua regia and the precious and base metals are determined using ICP mass spectrometry. Acme Analytical Laboratories in Vancouver, British Columbia, Canada, performed the ICP analyses.

XRD examinations were carried out in the Egyptian Geological Surveys Central Laboratories in Cairo using ZAF correction parameters; the operating conditions were 20 kV accelerating potential. The samples were examined using a scanning electron microscope (SEM–EDX) at Egyptian Geological Surveys Central Laboratories in Cairo, which used an SEM Model Quanta 250 FEG (Field Emission Gun) attached to an EDX Unit (Energy Dispersive X-ray Analyses), with an accelerating voltage of 30 kV, magnification of ×14 up to 1,000,000, and resolution of Gun.1n.

5 RESULTS

5.1 Petrography

Serpentinite is the most important rock unit of the ophiolite group in this region. These rocks are altered to talc-carbonates and listwaenite (quartz-carbonate).

Serpentinites consist principally of serpentine minerals (antigorite and chrysotile) with a minor amount of carbonates, talc, and opaque minerals (chromite). Serpentine minerals are mostly antigorite and chrysotile. Antigorite often occurs as colorless flaky, anhedral, and feather-shaped aggregates and sometimes as elongate blades with the roughly parallel arrangements (**Figure 4A**). Chrysotile forms colorless slip and crosses fiber veinlets (**Figure 4B**). Carbonate is present as an

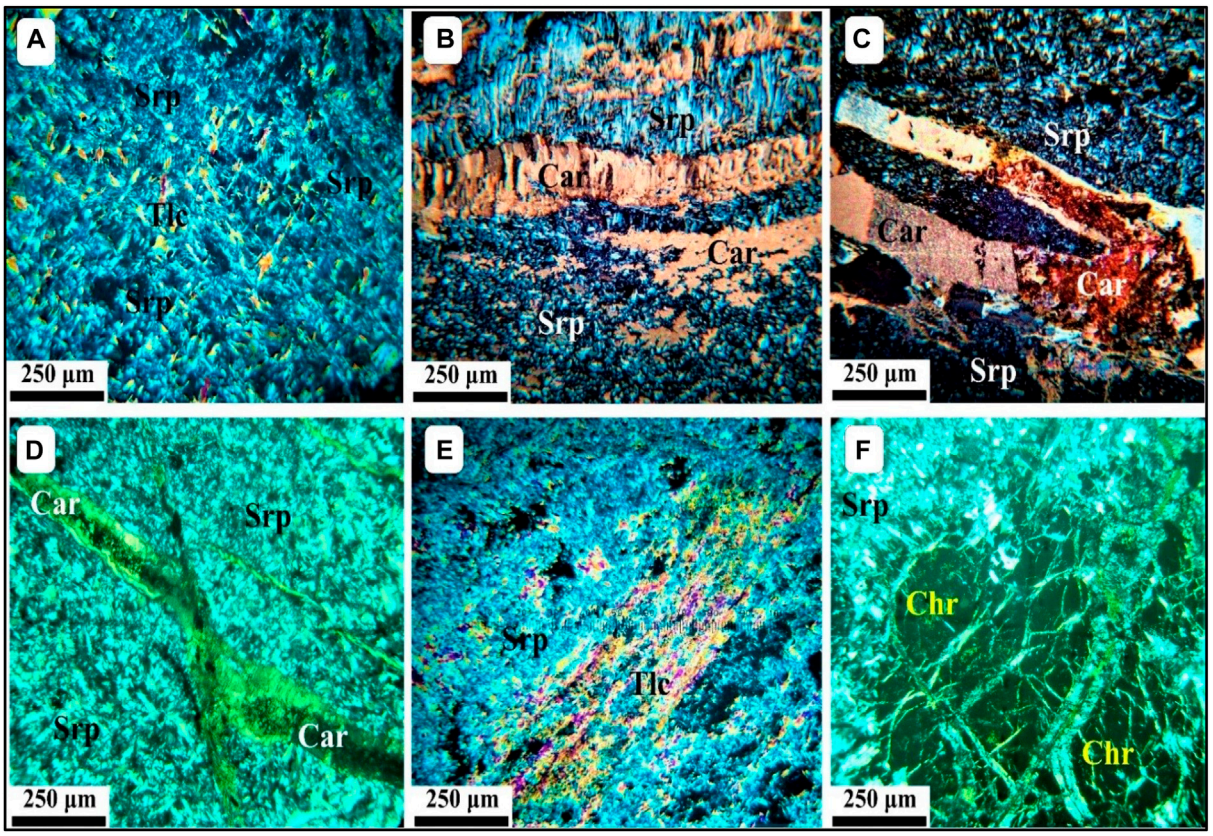

FIGURE 4 | Petrographical features of serpentinite rocks showing: **(A)** Non-pseudomorphic interpenetrating texture in serpentinites consisting of optically distinguishable blades of antigorite (Srp) minerals and talc (Tlc). C. N. **(B)** Serpentine (Srp) minerals altered to carbonate (Car). C. N. **(C)** Two types of carbonates (Car). C. N. **(D)** Bent of carbonate (Car) result of deformation. C. N. **(E)** Serpentine (Srp) minerals altered to talc (Tlc). C. N. **(F)** Coarse anhedral fractured chromite (Chr) crystal. C. N.

alteration product of serpentine minerals (**Figure 4B**) and occurs as fine-grained aggregates or patches and sometimes exists in microveinlet-like shapes (**Figure 4C**). In some parts, carbonates coalesce to form bent veinlets as a result of deformation (**Figure 4D**). Talc forms colorless fine-grained fibrous aggregates of parallel arrangement. It ranges in size from fine-grained scales and flakes to medium-grained cleaved plates (**Figure 4E**). Opaques are mainly chromite crystals, found filling the cracks and fractures; they are fractured with bloody red-colored core (**Figure 4F**).

Talc carbonates are dark greenish-gray to light gray or creamy in color. They are composed of equal proportions of talc and carbonate, with minor amounts of opaques. Talc occurs as a secondary mineral, formed by alteration of magnesium carbonates (magnesite and dolomite) and silicates as serpentine, tremolite, and chlorite (**Figure 5A**). Carbonates occur either as clusters, sparse patches, lenses, or veinlets embedded in talc (**Figure 5A**).

According to the present study, listwaenites are massive to semi schistose, and fine-grained rocks. Furthermore, as compared to the surrounding rocks, these rocks are more resistant to weathering. Along the Wadi Tilal Al-Qulieb area, listwaenites are distinguished into two main types based on the degree of alteration: i) silica-rich listwaenite, and ii) carbonate-rich listwaenite. Microscopically, silica–carbonate-rich listwaenite (types are much less widespread and partly envelops type 2 carbonate rich listwaenite. Petrographically, this type is composed of fine to coarse grains of quartz-dominated and contain a medium percent of carbonate. Quartz appears as xenomorphic to subidiomorphic crystals with undulose extinction consisting of fibrous aggregates and accessory minerals represented by iron oxides and graphite. Quartz and magnesite can also result from the reaction of talc and CO_2-rich fluids. Carbonation reactions and the influx of CO_2 can lead to quartz oversaturation and its co-precipitation with magnesite. Also, they contain a relict serpentinite fragment.

On the other hand, carbonate-rich listwaenite (type 2) is distinguished by the prevalence of carbonates, followed by the emergence of quartz. These rocks are composed of two phases of carbonates; the first phase is represented by coarse-grained aggregates or patches having pronounced twinkling and strong birefringence (**Figure 5B**), the second carbonate phase, exists in the form of lenses and kink banding (**Figure 5B**). Calcite is colorless, twinkled, and ranges from fine- to very coarse-grained

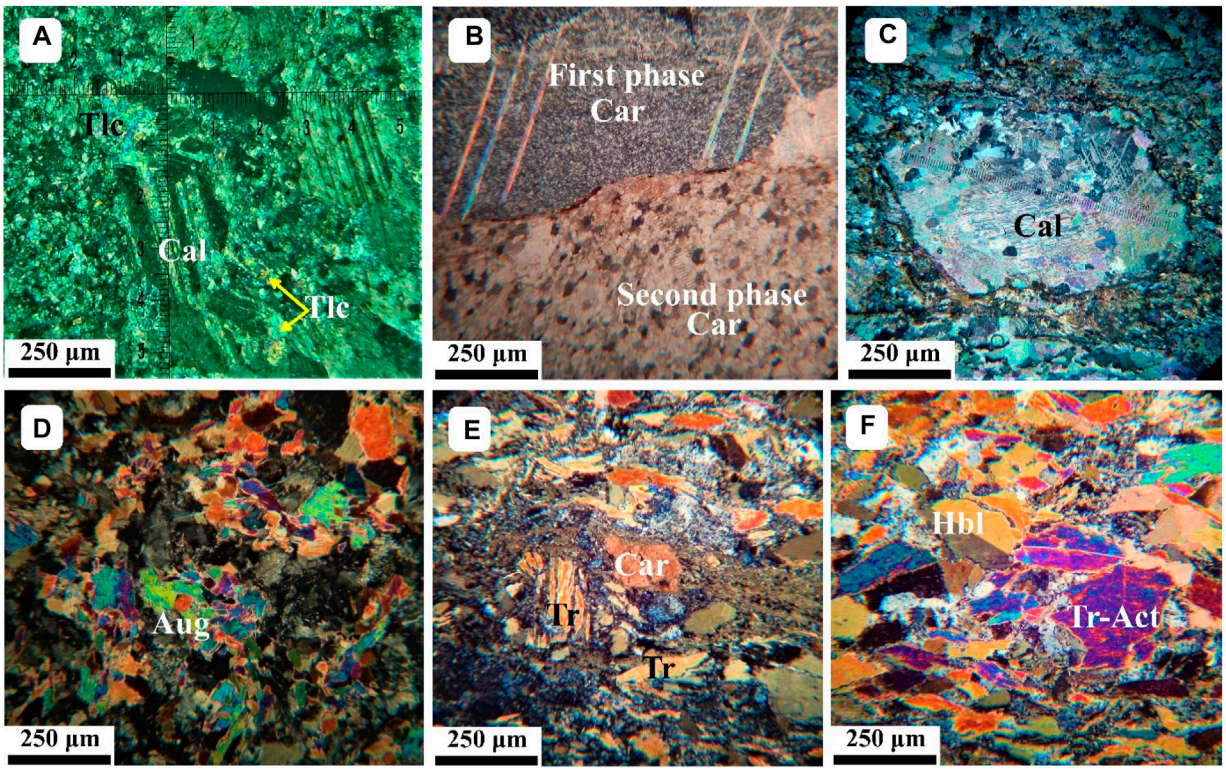

FIGURE 5 | Petrographical features of talc-carbonate, listwaenite, pyroxenite, and amphibolite rocks showing: **(A)** well-developed crystals of talc (Tlc) and calcite (Cal) crystals. C. N. **(B)** Showing two phases of carbonate deformation in listwaenite-like rock. C. N. **(C)** Mylonitization of larger carbonate (Car). C. N. **(D)** Green color augite (Aug) in pyroxenite rocks. C. N. **(E)** Sigmoid fish of immature carbonate (Car) and mylonitic texture in amphibolite. C. N. **(F)** Tremolite-actinolite crystal (Tr-Act) and Baveno twinning of hornblende (Hbl). C. N.

and is classified into two types: mature and immature crystals (**Figures 5B, C**). This type has been distinguished by granoblastic texture and frequently hosted a gold.

Pyroxenite occurs as unmappable pockets, lenses, or shear pods within the ultramafic rocks. These rocks are showing a granular texture. They are composed of augite, tremolite, actinolite, hornblende, talc, carbonates, and zoisite. They are composed mainly of sub-idiomorphic to xenomorphic clinopyroxene (augite) crystals. Augite crystals are characterized by high interference colors and partly to totally altered to hornblende and tremolite-actinolite (**Figure 5D**). Tremolite-actinolite occurs as idiomorphic to xenomorphic fine to medium-sized crystals, exhibiting a brown color of weakly pleochroism. Zoisite is found as short patches of allotriomorphic crystals after hornblende appears in blue interference colors and is usually associated with mafic minerals as a result of alteration processes. Talc and carbonates exist as secondary minerals and occur in veinlets cutting through the pyroxenites.

Amphibolites are unmappable massive, fine-grained to medium, and black to dark green in color. They are the diagnostic rocks of the amphibolite facies, and they are among the commonest rocks formed by regional metamorphism of moderate-to-high grade. They are composed mainly of tremolite-actinolite with occasion hornblende, calcite as well as zoisite and clinopyroxene. It is characterized by hypidiomorphic to xenoblast texture. Immature carbonate crystals are displayed as fish sigmoidal and mylonitic shapes (**Figures 5E, F**).

5.2 Geochemical Characteristics

Thirteen samples of the ophiolitic ultramafic rocks represented by serpentinites (four samples), amphibolites (three samples), listwaenites (four samples), and talc-carbonate rocks (two samples) were analyzed to determine their geochemical characteristics and origin (**Tables 1**, **2**). The investigated ophiolitic rocks show that the SiO_2 contents range from 1.95% to 57.49 wt%. The low SiO_2 value is recorded in the talc carbonate rocks and the highest values are recorded in listwaenites attributed to high quartz contents in these rocks.

The lowest Al_2O_3 values (0.08%–0.43 wt%, respectively), were recorded in talc carbonate rocks and serpentinites. The values of Al_2O_3 increase in amphibolite and listwaenites (16.02% and 12.45 wt% respectively). The high CaO values (33.45 wt%) encountered in the talc carbonate rocks point to high calcite content. CaO content is high in the ophiolite assemblage due to the alteration of the mafic minerals into carbonate minerals. Furthermore, the CaO values of serpentinites range from 0.34% to 3.36 wt% with an average of 1.69 wt%. MgO contents range from 39.56% to 40.73 wt%. The highest MgO values (40.73 wt%) recorded in the serpentinites were attributed to the serpentine

TABLE 1 | Chemical composition of the Tilal Al qulieb serpentinite and amphibolite rocks.

	Major elements (wt%)								
	Serpentinite					Amphibolite			
S.No.	**31**	**32**	**33**	**35**	**Ave**	**22**	**23**	**24**	**Ave**
SiO_2	38.51	35.3	38.86	35.09	**36.69**	45.13	38.4	45.27	**42.9**
TiO_2	0.0033	0.0017	0.0083	0.005	**0.005**	0.50	0.89	1.09	**0.82**
Al_2O_3	1.28	0.43	0.53	0.45	**0.67**	16.02	15.57	15.83	**15.47**
Fe_2O_3*	6.41	5.72	7.15	5.85	**6.28**	9.36	12.14	12.75	**11.41**
MnO	0.07	0.10	0.04	0.09	**0.07**	0.18	0.20	0.21	**0.19**
MgO	39.56	39.86	40.34	40.73	**40.12**	11.41	13.08	8.26	**10.91**
CaO	0.70	3.36	0.34	2.36	**1.69**	9.46	9.88	9.98	**9.77**
Na_2O	0.01	0.04	0.01	0.02	**0.02**	2.35	2.08	2.77	**2.4**
K_2O	0.01	0.01	0.01	0.01	**0.01**	0.37	0.13	0.08	**0.19**
P_2O_5	0.01	0.02	0.00	0.01	**0.01**	0.09	0.01	0.09	**0.06**
L.O.I	13.44	16.1	12.7	15.3	**15.4**	5.13	7.62	5.67	**5.80**
Total	100	100	100	100	**100**	100	100	100	**100**
	Trace elements (ppm)								
Cu	5.1	3.8	11.9	5.2	**6**	16.4	209.5	138.5	**121.4**
Pb	0.36	1.08	2.00	5.41	**2.21**	1.65	2.16	0.85	**1.5**
Zn	45.3	21.3	29.3	25.5	**30.35**	65.2	69.2	87.6	**73.6**
Ag	0.187	0.190	0.15	0.140	**0.16**	0.07	0.132	0.05	**0.08**
Ni	2095.1	2,316.4	1997.8	2,444	**2,213.3**	52.5	243.4	122.8	**139.5**
Co	105.0	99.8	93.6	102.6	**100**	65.4	87.2	60.2	**70.9**
U	<0.1	<0.1	<0.1	<0.1	**0.1**	0.1	<0.1	<0.1	**0.03**
Th	<0.1	<0.1	<0.1	<0.1	**0.1**	0.2	<0.1	0.2	**0.13**
Sr	6	23	3	30	**15.5**	160	240	131	**177**
Cd	0.10	0.12	0.08	0.10	**0.1**	0.08	0.25	0.08	**0.13**
V	21	17	21	18	**19.25**	194	342	300	**278.6**
Cr	1,386	703	918	933	**985**	317	310	284	**303.6**
Ba	20	11	6	17	**13.5**	199	58	36	**97.6**
Zr	0.3	0.3	0.3	0.3	**0.3**	**8.5**	**3.5**	**22**	**15.25**
Sc	5.3	7.0	5.3	5.6	**5.8**	49.3	40.3	45.1	**45.5**
Y	0.3	<0.1	0.3	0.1	**0.2**	12.0	6.3	19.7	**12.6**
Hf	<0.02	0.02	<0.02	<0.02	**0.02**	0.37	0.23	0.57	**0.39**
Li	0.3	0.5	0.2	0.4	**0.3**	11.6	21.0	15.5	**16.03**
Rb	<0.1	0.2	0.1	0.1	**0.1**	6.9	2.1	1.0	**3.33**
Ta	<0.1	<0.1	<0.1	<0.1	**0.1**	<0.1	<0.1	0.2	**0.06**
Nb	0.06	0.07	0.04	0.05	**0.05**	0.40	0.16	3.12	**1.22**
Cs	<0.1	<0.1	<0.1	<0.1	**0.1**	0.2	<0.1	<0.1	**0.066**
Ga	0.69	0.34	0.58	0.41	**0.5**	11.06	15.98	13.94	**13.32**
	Rare earth elements (ppm)								
La	0.2	0.1	0.1	0.1	**0.12**	2.2	1.1	3.7	**2.33**
Ce	0.42	0.20	0.19	0.19	**0.2**	5.13	2.32	9.15	**5.53**
Pr	<0.1	<0.1	<0.1	<0.1	**—**	0.7	0.3	1.6	**0.86**
Nd	0.2	<0.1	0.2	0.1	**—**	5.1	2.2	7.5	**5.6**
Sm	<0.1	<0.1	<0.1	<0.1	**—**	1.5	0.8	2.6	**1.63**
Eu	<0.1	<0.1	<0.1	<0.1	**—**	0.7	0.4	1.0	**0.7**
Gd	0.1	0.1	0.1	0.1	**—**	2.2	1.2	3.3	**2.23**
Tb	<0.1	<0.1	<0.1	<0.1	**—**	0.3	0.1	0.5	**0.3**
Dy	<0.1	<0.1	<0.1	<0.1	**—**	2.4	1.3	5.0	**2.56**
Ho	<0.1	<0.1	<0.1	<0.1	**—**	0.5	0.3	0.9	**0.56**
Er	<0.1	<0.1	<0.1	<0.1	**—**	1.4	0.8	2.5	**1.56**
Tm	<0.1	<0.1	<0.1	<0.1	**—**	0.2	0.1	0.3	**0.2**
Yb	0.1	0.1	0.1	0.1	**—**	1.2	0.7	2.2	**1.36**
Lu	<0.1	<0.1	<0.1	<0.1	**—**	0.2	0.1	0.3	**0.2**
ΣREE	0.82	0.2	0.49	0.29	**—**	22.73	11.7	39.55	**25.62**
ΣLREE	0.92	0.4	0.59	0.49	**—**	16.53	8.32	28.85	**17.8**
ΣHREE	0.1	0.1	0.1	0.1	**—**	6.2	3.4	10.7	**6.74**
$(La/Yb)_N$	1.36	0.66	0.66	0.66	**—**	1.26	1.06	1.15	**1.18**
$(Gd/Yb)_N$	0.79	0.79	0.79	0.79		1.48	1.39	1.21	**1.32**

TABLE 2 | Chemical composition of listwaenites and talc-carbonate rocks.

	Major elements (wt%)										
	Carbonate-rich listwaenites			**Silica–carbonate-rich listwaenites**				**Talc-carbonate**			
S. No.	**17**	**18**	**Q***	**45**	**46**	**Q****	**Q*****	**19**	**20**	**T***	**T****
SiO_2	38.25	30.21	**34.23**	35.26	57.49	**46.37**	**36.25**	1.95	34.21	**18.08**	**12.77**
TiO_2	0.05	0 0.08	**0.025**	0.48	0.33	**0.40**	**0.07**	0.00	0.03	**0.01**	**0.01**
Al_2O_3	14.59	12.45	**13.52**	14.13	14.08	**14.10**	**1.30**	0.08	16.91	**8.49**	**0.70**
FeO	0.91	1.08	**0.99**	0.83	0.56	**0.69**	**4.86**	0.02	0.93	**0.47**	**1.64**
Fe_2O_3*	9.08	10.81	**9.94**	8.29	5.60	**6.94**	**5.40**	0.16	9.31	**4.73**	**0.79**
MnO	0.13	0.15	**0.14**	0.21	0.11	**0.16**	**0.67**	0.01	0.13	**0.07**	**0.48**
MgO	14.58	17.91	**16.24**	12.17	4.08	**8.12**	**13.56**	17.78	26.37	**22.07**	**11.07**
CaO	5.32	8.28	**6.8**	13.91	5.09	**9.5**	**16.01**	33.45	0.24	**16.8**	**36**
Na_2O	1.98	0.14	**1.06**	1.80	2.10	**1.95**	**0.21**	0.01	0.02	**0.01**	**0.05**
K_2O	0.49	0.06	**0.27**	0.29	2.59	**1.44**	**0.29**	<0.01	<0.01	**0**	**0.06**
P_2O_5	0.02	0.03	**0.02**	0.03	0.17	**0.1**	**0.03**	0.14	0.05	**0.09**	**0.01**
L.O.I	14.6	18.8	**16.7**	12.6	7.8	**10.2**	**26.64**	46.4	11.8	**29.1**	**36**
Total	100	100	**100**	100	100	**100**	**99.52**	100	100	**100**	**99.90**
	Trace elements (ppm)										
Cu	2.6	18.0	**10.3**	22.0	21.7	**21.85**	**257**	0.5	0.4	**0.45**	**—**
Pb	5.20	3.21	**4.20**	2.69	10.93	**6.81**	**153**	1.48	0.70	**1.09**	**22**
Zn	71.5	118.8	**95.15**	55.6	74.4	**65**	**90**	18.6	58.4	**38.5**	**29**
Ag	0.100	0.124	**0.11**	0.041	0.057	**0.049**	**—**	0.137	0.111	**0.124**	**—**
Ni	438.5	979.3	**708.9**	281.3	91.6	**186.4**	**834**	3.1	464.3	**233.7**	**795**
Co	79.8	117.9	**98.85**	52.8	17.9	**35.35**	**47**	0.7	67.1	**33.9**	**27**
U	<0.1	0.2	**0.1**	<0.1	1.5	**0.75**	**—**	0.2	0.1	**0.15**	**1**
Th	<0.1	0.2	**0.1**	0.3	8.2	**4.25**	**—**	<0.1	0.3	**0.15**	**4**
Sr	177	172	**174.5**	324	111	**217.5**	**404**	206	4	**105**	**120**
Cd	0.07	0.13	**0.1**	0.10	0.13	**0.115**	**—**	0.27	0.03	**0.15**	**—**
V	105	146	**125.5**	125	80	**102.5**	**34**	2	110	**56**	**25**
Cr	838	1,534	**1,186**	528	103	**315.5**	**351**	6	102	**54**	**1,035**
Ba	67	21	**44**	113	728	**420.5**	**94**	7	2	**4.5**	**64**
W	<0.1	0.1	**0.05**	0.1	0.7	**0.4**	**—**	0.1	<0.1	**0.05**	**—**
Zr	3.4	6.9	**5.15**	2.9	95.3	**49.1**	**34**	1.8	28.0	**14.9**	**7**
Sn	0.2	0.2	**0.2**	0.2	1.3	**0.75**	**—**	<0.1	0.1	**0.05**	**—**
Sc	23.4	19.2	**21.3**	36.3	10.1	**23.2**	**—**	0.6	5.1	**2.85**	**—**
Y	1.6	2.5	**2.05**	7.7	11.5	**9.6**	**2**	4.9	1.2	**3.05**	**5**
Hf	0.15	0.23	**0.19**	0.17	2.72	**1.44**	**—**	0.06	0.89	**0.47**	**—**
Li	107.6	61.9	**84.75**	27.3	38.5	**32.9**	**—**	0.8	28.9	**14.85**	**—**
Rb	10.4	1.8	**6.1**	5.5	86.2	**45.85**	**16**	0.2	0.2	**0.2**	**4**
Ta	<0.1	<0.1	**0**	<0.1	0.2	**0.1**	**—**	<0.1	<0.1	**0**	**4**
Nb	0.11	0.27	**0.19**	0.39	3.64	**2.01**	**13**	0.10	0.04	**0.07**	**5**
Cs	0.6	0.3	**0.45**	<0.1	4.2	**2.1**	**—**	<0.1	<0.1	**0**	**—**
Ga	12.77	14.36	**13.56**	14.09	14.84	**14.46**	**—**	0.07	14.30	**7.18**	**34**
	Rare earth elements (ppm)										
La	1.4	1.8	**1.6**	1.6	34.2	**17.9**	**—**	2.5	1.2	**1.85**	**1.5**
Ce	2.75	3.36	**3.055**	3.51	65.6	**34.55**	**—**	2.91	3.08	**2.99**	**4**
Pr	0.3	0.4	**0.35**	0.5	7.8	**4.15**	**—**	0.5	0.4	**0.45**	**—**
Nd	1.8	2.4	**2.1**	2.6	27.5	**15.05**	**—**	1.9	2.1	**2**	**—**
Sm	0.6	0.7	**0.65**	0.9	4.9	**2.9**	**—**	0.4	0.6	**0.5**	**—**
Eu	0.3	0.4	**0.35**	0.5	1.1	**0.8**	**—**	<0.1	<0.1	**0**	**—**
Gd	0.4	0.7	**0.55**	1.3	4.4	**2.85**	**—**	0.5	0.4	**0.45**	**—**
Tb	<0.1	<0.1	**0**	0.2	0.5	**0.35**	**—**	<0.1	<0.1	**0**	**—**
Dy	0.3	0.5	**0.4**	1.5	2.5	**2**	**—**	0.4	0.3	**0.35**	**—**
Ho	<0.1	<0.1	**0**	0.3	0.4	**0.35**	**—**	0.1	<0.1	**0.05**	**—**
Er	0.2	0.4	**0.3**	0.9	1.3	**1.1**	**—**	0.3	0.2	**0.25**	**—**
Tm	<0.1	<0.1	**0**	0.1	0.2	**0.15**	**—**	<0.1	<0.1	**0**	**—**
Yb	0.3	0.3	**0.3**	0.7	1.4	**1.05**	**—**	0.2	0.2	**0.2**	**—**
Lu	<0.1	<0.1	**0**	0.1	0.2	**0.15**	**—**	<0.1	<0.1	**0**	**—**
ΣREE	8.35	10.96	**9.655**	14.71	152	**83.35**	**—**	9.71	8.48	**9.09**	**5.5**
ΣLREE	7.55	9.76	**8.655**	10.91	145.5	**78.2**	**—**	8.71	7.78	**8.24**	**5.5**
ΣHREE	0.8	1.2	**1**	3.8	6.5	**5.15**	**—**	1	0.7	**0.85**	**—**
$(La/Yb)_N$	3.16	4.08	**3.58**	1.54	0.01	**11.52**	**—**	8.5	4.07	**6.3**	**—**
$(Gd/Yb)_N$	1.08	1.9	**1.49**	1.50	2.54	**2.20**	**—**	2.03	1.62	**1.83**	**—**

Q = Average of Wadi Umm Ashira listwaenites. T* = average of the studied talc-carbonate rocks.*

*Q** = Average of Wadi Tilal Al-Qulieb listwaenites. T** = Average of El-Zarieb talc-carbonate rocks (Shaheen, 2012).*

*Q*** = Average of Wadi Garf listwaenites (El-Desoky and Saleh, 2012).*

Bold values represent the average values.

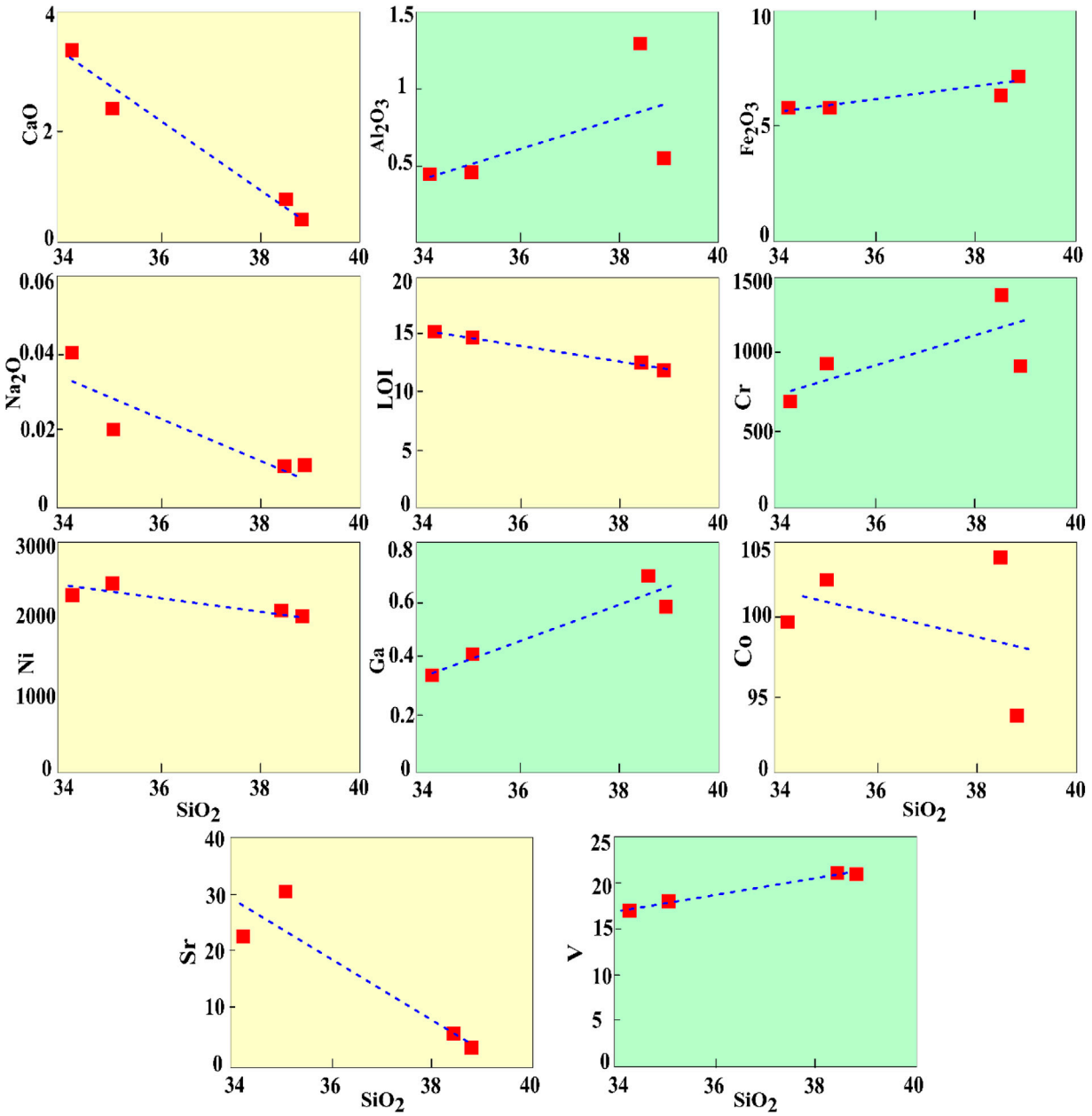

FIGURE 6 | Major and trace element versus SiO_2 bivariate plots for the serpentinite samples.

minerals and the lowest MgO contents were observed in the listwaenite rocks (4.08 wt%).

5.2.1 Geochemical Results of Serpentinites

The relation between SiO_2 and major oxides exhibits a negative correlation with CaO, Na_2O, LOI, Ni, and Sr (as these elements decrease with increasing SiO_2 content; **Figure 6**). Meanwhile, Al_2O_3, Fe_2O_3*, Ga, V, and Cr show a positive correlation (i.e., increase with increasing SiO_2 contents). All the analyzed serpentinites show high LOI (Loss on Ignition) values, from 12.7% to 16.1 wt%, reflecting the high degree of serpentinization.

Serpentinites have a low amount of Al (0.43%–1.28 wt%), while having a large range of MgO concentration (from 39.56% to 40.73 wt%, **Table 1**), which might be due to a variety of protolith fertility or Mg during low-temperature seabed alteration (Snow and Dick, 1995; Niu, 2004). $Fe_2O_3^*$ concentrations vary from 5.72% to 7.15 wt%.

The serpentinization and associated carbonation processes are known to have a significant impact on whole-rock CaO concentration (Miyashiro et al., 1969; Coleman and Keith, 1971; Janecky and Seyfried, 1986; Palandri and Reed, 2004). The high MgO/LOI ratio is a

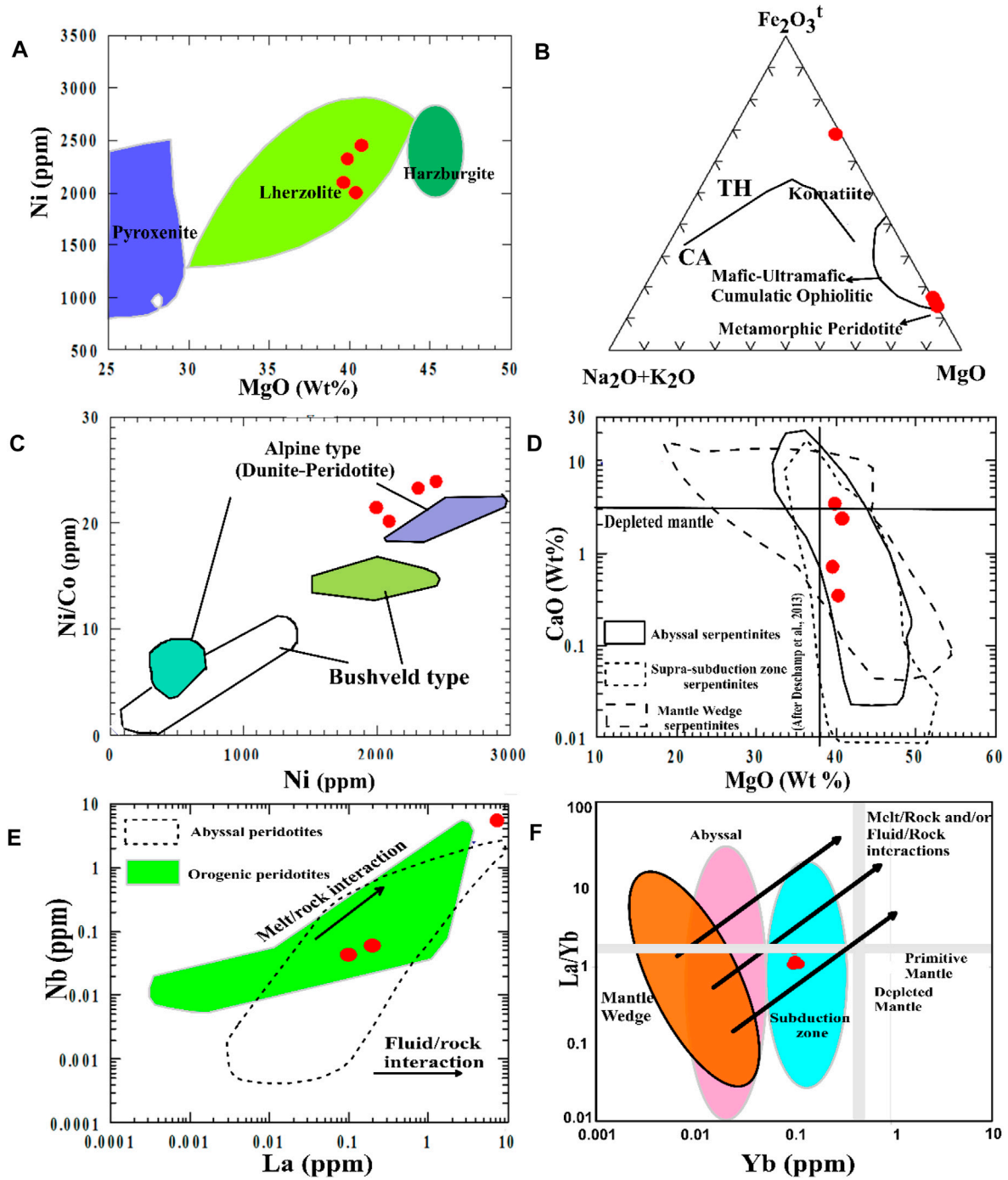

FIGURE 7 | (A) Variation diagrams of Ni versus MgO in the serpentinite rocks (Pfeifer, 1990). **(B)** $Fe_2O_3^t$–(Na_2O + K_2O)–MgO ternary diagrams after Coleman (1977). **(C)** Ni/Co versus Ni diagrams in comparison with ratios of alpine-type and Bushveld-layered ultramafics (Gulacar and Delalaye, 1976. **(D)** CaO versus MgO plots for serpentinite. Mg number lines (Deschamps et al., 2013) and depleted mantle after Workman and Hart (2005). **(E)** Nb versus La binary diagram after Paulick et al. (2006) and abyssal peridotites from Paulick et al. (2006), Deschamps et al. (2013) as well as orogenic and ophiolitic peridotites from Bodinier and Godard (2003). **(F)** La/Yb ratio versus Yb contents (ppm) for serpentinites after Deschamps et al. (2013).

good sign of dolomitization and carbonization processes. Carbonization begins when CO_2^--rich fluids interact with sensitive rocks in the crust and mantle, resulting in the alteration and precipitation of carbonate and other minerals. The significant carbonization of the ophiolite units implies a high circulation of CO_2^-bearing fluid.

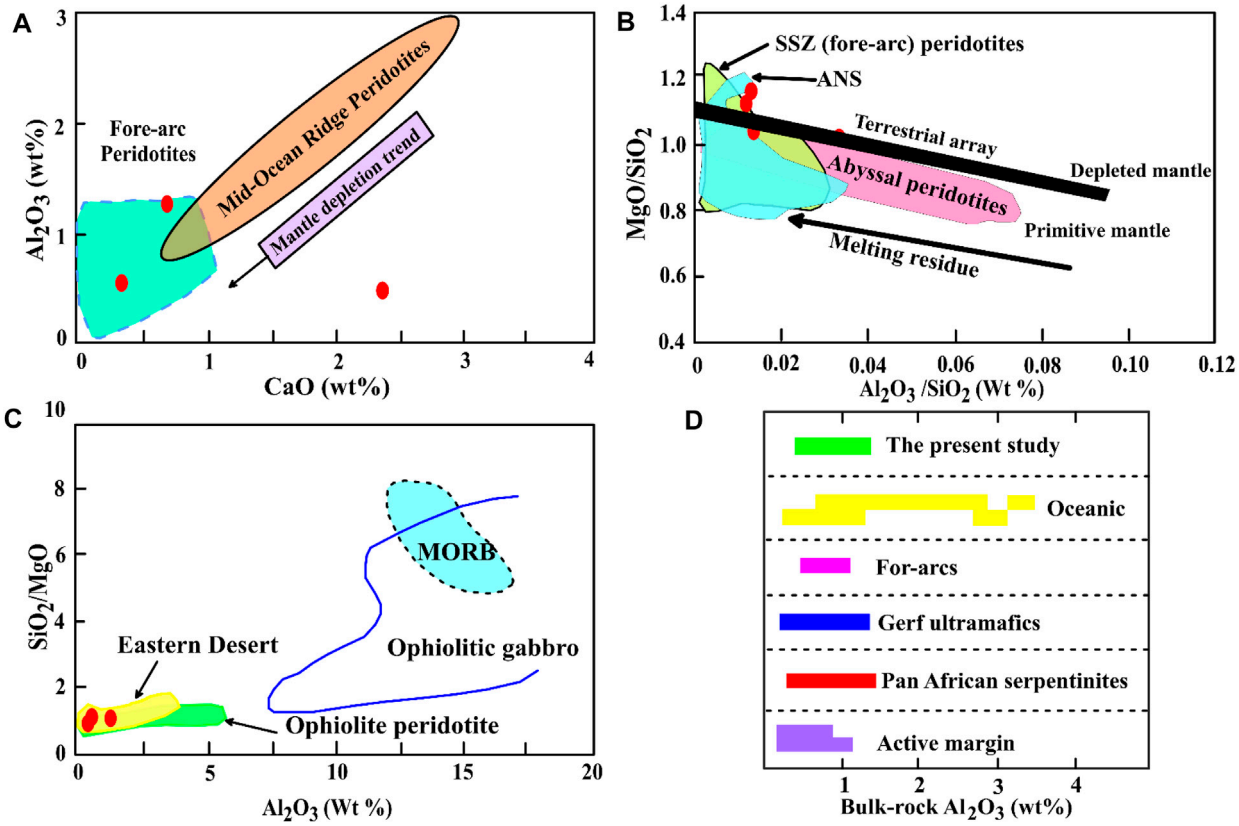

FIGURE 8 | (A) CaO versus the Al_2O_3 diagram showing KUS serpentinites compared with forearc and MOR peridotites (Ishii et al., 1992). **(B)** MgO/SiO_2 versus Al_2O_3/SiO_2 diagram. Primitive and depleted mantle values are from McDonough and Sun (1995) and Salters and Stracke (2004), respectively. The "terrestrial array" represents the bulk silicate Earth evolution (Jagoutz et al., 1979; Zindler and Hart, 1986). Fields of abyssal and forearc peridotites are after Parkinson and Pearce (1998), Pearce et al. (2000), and Niu (2004). ANS ophiolitic peridotite field is after Ahmed and Habtoor (2015) and Abdel-Karim et al. (2018). **(C)** SiO_2/MgO ratios versus the Al_2O_3 diagram. Fields of ophiolitic gabbros and peridotites, as well as MORB are from Bodinier and Godard (2003). Data from the Eastern Desert are shown for comparison by Zimmer et al. (1995); Azer and Khalil (2005), Azer and Stern (2007), Azer et al. (2013), Abdel-Karim et al. (2016) and Abdel-Karim et al. (2018). **(D)** Bulk-rock Al_2O_3 (wt%) contents of Tilal Al-Qulieb serpentinites compared with those from different tectonic settings and the Pan-African serpentinites.

5.2.1.1 Nature of the Serpentinites (Protoliths)

According to the variation diagram of Ni versus MgO after Pfeifer (1990), the serpentinite samples plot on the lherzolite field (**Figure 7A**). According to $Fe_2O_3^t$-(Na_2O + K_2O)-MgO ternary diagrams after Coleman (1977), the serpentinite samples plot in the metamorphic peridotite field (**Figure 7B**). Based on the binary diagram (Ni/Co versus Ni) after Gulacar and Delalaye (1976), the serpentinite samples fall close to the Alpine type field (Dunite-Peridotite; **Figure 7C**).

5.2.1.2 Geotectonic Environments and Petrogenesis of the Serpentinites

On the CaO versus MgO binary diagram (**Figure 7D**), the present serpentinites plot in the overlap zone between abyssal serpentinite, supra-subduction zone serpentinites, and mantle wedge serpentinites toward the depleted mantle side (Lines are after Deschamps et al., 2013 and depleted mantle after Workman and Hart, 2005).

The plots of incompatible trace elements on the Nb versus La binary diagrams were revealed in **Figure 7E**. Arrows relating to fluid-rock and melt-rock interactions from Paulick et al. (2006), the compositional field for abyssal peridotites from Paulick et al. (2006), and Deschamps et al. (2013) as well as orogenic and ophiolitic peridotites from Bodinier and Godard (2003). According to Deschamps et al. (2013) (La/Yb versus Yb diagram), the studied serpentinite samples were plotted in the subduction zone (**Figure 7F**).

Most Eastern Desert ophiolites are thought to have originated in a supra-subduction zone (SSZ), which means they are formed, by the sea bottom extending over an active subduction zone (Abu El-Ela, 1996; El-Sayed et al., 1999; Stern et al., 2004; Azer and Khalil, 2005; Azer and Stern 2007; Abdel-Karim et al., 2016). Regardless, whether these SSZ ophiolites were deposited in a forearc or backarc context is a point of contention.

The Al_2O_3 and CaO binary graphs are reduced in Al_2O_3 and CaO, and equivalent to fore-arc settings (**Figure 8A**), according to Ishii et al. (1992). They overlap both abyssal and fore-arc peridotites (**Figure 8B**). On the SiO_2/MgO versus Al_2O_3 diagram (**Figure 8C**); they are affiliated with ophiolitic peridotites as do the other Eastern Desert ophiolitic ultramafics. The investigated serpentinites differ significantly from those found elsewhere as seen in **Figure 8D**. Low Al_2O_3 abundances (0.43%–1.28%) define

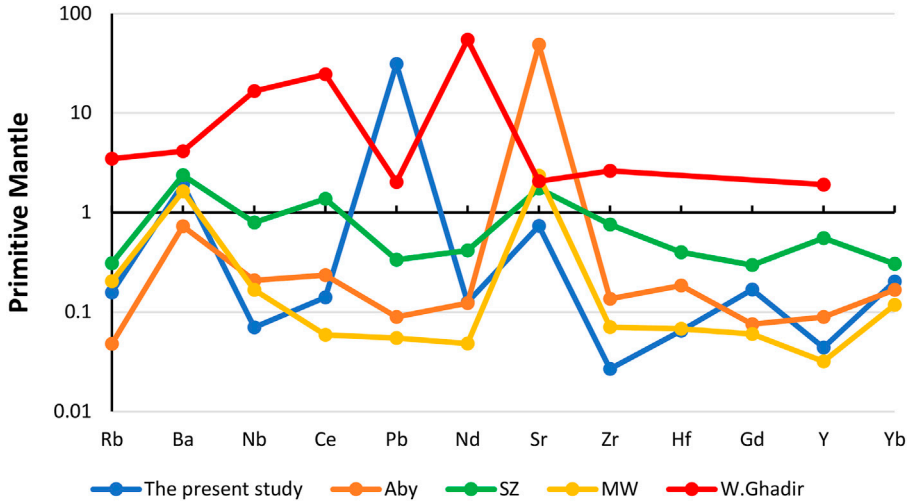

FIGURE 9 | Primitive mantle-normalized patterns (according to Sun and McDonough, 1989) of trace and REE in the studied serpentinites showing a comparison between the present studied, Wadi Ghadir after Surour (2017), and an average of abyssal, SZ and mantle wedge after Deschamps et al. (2013).

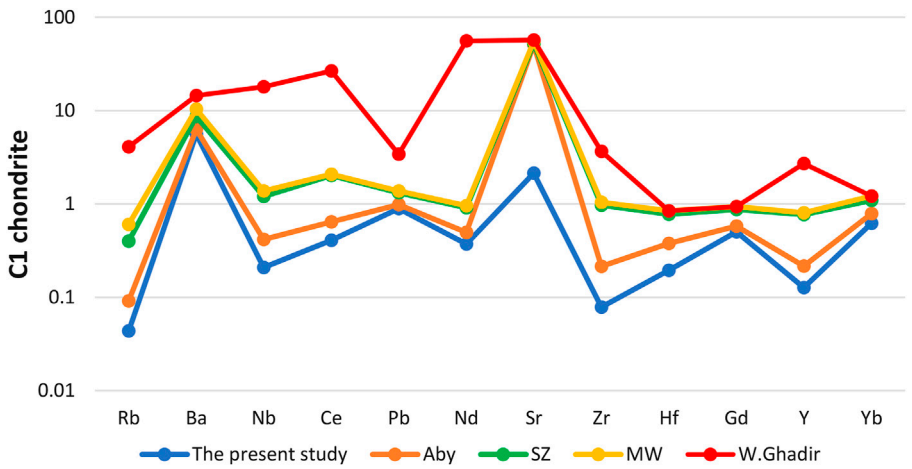

FIGURE 10 | C1-chondrite-normalized patterns (according to McDonough and Sun, 1995) of trace and REE in the studied serpentinites showing a comparison between the present study, Wadi Ghadir after Surour (2017) and average of abyssal, SZ, and mantle wedge after Deschamps et al. (2013).

the investigated serpentinites, which are similar to peridotites from contemporary for-arcs and Neoproterozoic serpentinized peridotites from the Eastern Desert, Egypt (**Figure 8D**).

The plots in **Figure 9** clearly show that the studied serpentinite samples are plotted in the overlap zone between abyssal and orogenic peridotites. **Figures 9**, **10** show the distribution of trace elements normalized to the primitive upper mantle (Sun and McDonough, 1989; McDonough and Sun, 1995) for the present serpentinites, and compared with Wadi Ghadir after Surour (2017), and an average of abyssal, subduction zone, and mantle wedge after Deschamps et al. (2013).

5.2.2 Geochemical Results of Amphibolites

The studied amphibolite shows variable ranges in their chemical composition either for major oxides and or trace elements. The SiO_2 varies from 38.4% to 45.27% with an average (42.9%), $A1_2O_3$ varies from 15.83% to 16.02% with an average 15.47%, MgO varies from 8.26% to 13.08% with an average 10.91%, and CaO varies from 9.46% to 9.98% with an average of 9.77% (**Table 1**). The average LOI values, total alkali ($Na_2O + K_2O$), TiO_2, MnO, and P_2O_5 are 5.66%, 2.59%, 0.82%, 0.19%, and 0.06%, respectively (**Table 1**). The average trace elements contents of V, Cr, Ni, Sr, and Cu are (278.6, 303.6, 139.5, 177, and 121.4 ppm, respectively). The average of other trace elements are: Pb (1.5 ppm), Zn (73.6 ppm), Co (70.9 ppm), U (0.03 ppm), Th (0.13 ppm), Zr (0.1 ppm), Y (12.6 ppm), Li (16.03 ppm), Rb (3.33 ppm), and Ga (13.32 ppm, **Table 1**).

On the Al_2O_3–CaO–MgO ternary diagram (**Figure 11A**) of Coleman (1977), amphibolite samples plot in the mafic cumulate field associated with MORB. The relation between Co and Ni

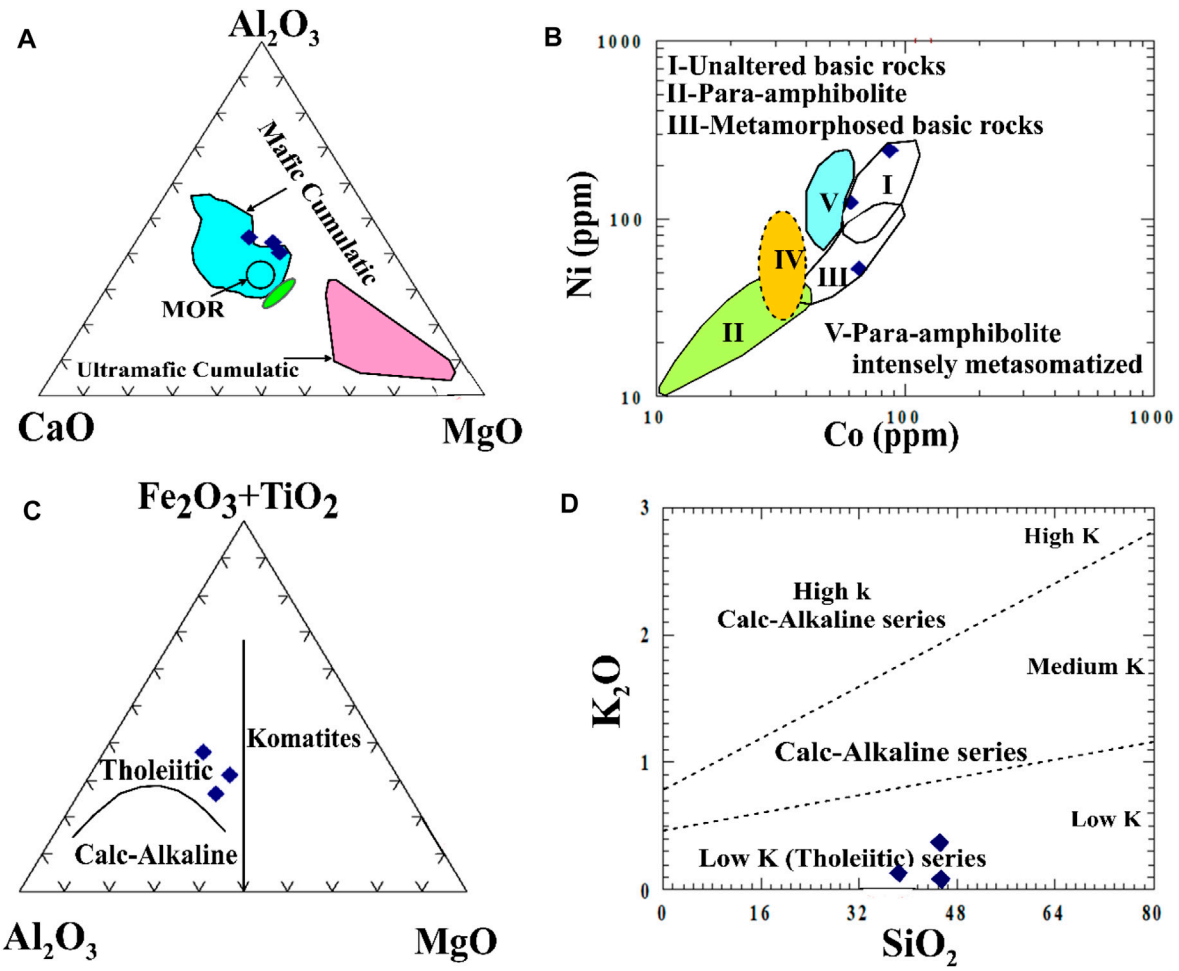

FIGURE 11 | (A) Al_2O_3-CaO-MgO ternary diagram for the amphibolite rocks (Coleman, 1977). **(B)** Ni versus Co for the present amphibolites rocks after Walker et al. (1960) and Heier (1960). **(I)** unaltered and slightly altered basic magmatic rocks. **II-**Para-amphibolites of low to moderate grade alteration, including metasomatism. **III-** metamorphosed basic magmatic rocks (metadolerites and metabasalts). **IV-** Ortho-amphibolites intensely metasomatized. **V-** Para-amphibolites, intensely metasomatized. **(C)** (Fe_2O_3+ TiO_2)–Al_2O_3 MgO diagram for the studied amphibolite rocks (Jensen, 1976). **(D)** K_2O versus SiO_2 binary diagram for amphibolite rocks (Le maitre et al., 1989).

of Walker et al. (1960) and Heier (1960) illustrates that the present amphibolite was derived from unaltered to slightly altered basic magmatic rocks to metamorphosed basic rocks (**Figure 11B**).

The (Fe_2O_3+ TiO_2)–Al_2O_3–MgO ternary diagram of Jensen (1976) illustrates the nature of the primary magma of the ultramafic rocks. In this diagram, the amphibolite samples plot in the tholeiitic field (**Figure 11C**). Le maitre et al. (1989) classified the different magma types into three series depending on the potassic ratio. The present amphibolite rocks plot in the low-K tholeiitic series field (**Figure 11D**).

5.2.3 Geochemical Results of Listwaenites and Talc-Carbonate Rocks

Representative chemical analyses of four rock samples of listwaenites and two samples of talc-carbonate rocks are given in **Table 2**. Listwaenites and talc-carbonate rocks were considered as alteration products of serpentinites (El-Desoky and Khalil, 2011 and El-Desoky and Saleh, 2012). The studied listwaenites demonstrated high contents of SiO_2 (30.21%–57.49%), CaO (5.09%–13.91%), Al_2O_3 (12.45%–15.59%), Fe_2O_3 (5.60%–10.81%), MgO (5.08%–17.91%), and LOI (7.8%–18.8%), and low concentrations of TiO_2 (0.05%–0.48%), MnO (0.11%–0.21%), and P_2O_5 (0.02%–0.17%), (**Table 2**). Other major elements showed low and moderate variations: Na_2O (0.14%–2.10%) and K_2O (0.06%–2.59%). SiO_2, MgO, CaO, Al_2O_3, and Fe_2O_3 are the most variable major oxides that are mobilized during different phases of alteration. Volatile components are reported as a loss on ignition (LOI) and can be used as a measure of the degree of serpentinization or listwaenitization. The LOI value increases with increasing the intensity of carbonatization. Trace element analyses demonstrated high contents of Cr (528–1,534 ppm), Ni (281.3–979.3 ppm), and Co (79.8–117 ppm). Regarding the

talc-carbonate rocks, the most variable elements are of SiO_2 (35.21%), MgO (26.37%), CaO (33.45%), (16.91%), Fe_2O_3 (9.31%), and Ni (465.3%).

Ultramafic rocks consist of ferro-magnesian silicate minerals. Anhydrous ultramafic rocks contain olivine, orthopyroxene, and calcic clinopyroxene in various proportions. Consequently, Bucher and Grapes (2011) demonstrated the system components: SiO_2, FeO, MgO, and CaO constitute more than 95% of almost anhydrous ultramafitites. Iron represents an important component in most ultramafic rocks. Bucher and Grapes (2011) used the system SiO_2–MgO–CaO- for a discussion of the metamorphism of ultramafic rocks. **Figures 13A, B** show the chemography of the CMS system of the studied listwaenites and talc-carbonate rocks and imply typical ultramafic rocks and mineral compositions. According to the SiO_2–CaO–MgO ternary diagram (Bucher and Grapes, 2011), the listwaenite samples trend toward rich tremolite and quartz, while the talc carbonate rocks plot on the talc and calcite-dolomite axis (**Figure 13A**).

The SiO_2–CaO–MgO diagram (Bucher and Grapes, 2011) shows the listwaenites samples with a slight tendency to be of tremolite and silica in nature, while talc carbonate samples falling in talc and (calcite-dolomite), (**Figure 13A**). All three carbonate minerals, calcite, dolomite, and magnesite in **Figure 13B** occur in ultramafic rocks.

6 DISCUSSION

6.1 Petrogenesis of the Ophiolitic Ultramafic Rocks

The chemical composition of the studied serpentinites (**Table 1**) compared to El-Rubshi serpentinites (El-Desoky et al., 2015) show lower contents of FeO, Na_2O, K_2O, P_2O_5, and LOI, as well as Mo, U, Th, Bi, Cr, W, Zr, CO, Ni, Rb, Hf, Nb, and Ta. Meanwhile, the studied serpentinites were distinguished by extraordinary higher contents of SiO_2, Fe_2O_3, CaO, Cu, Zn, Sr, V, Ba, Y, and Ga.

The normalized spider diagram (**Figure 9**) of the investigated serpentinites is represented, according to the primitive mantle of McDonough and Sun (1989). From this diagram, it is clear that there is noticeable depletion of Ce, Nd, Zr, and Y. The trace elements and REE concentrations from Tilal Al-Qulieb and Wadi Ghadir serpentinites (Surour, 2017) are normalized to the composition of the chondrite (C1) rocks described by McDonough and Sun (1995); **Figure 10**). It is clear from the diagram that the studied rocks show depletion in Rb, Nb, Nd, Zr, and Y, with respect to the chondrite (C1) abundances and also show relative enrichment in Ba, Ce, and Sr.

In general, we will compare the chemical analysis of the studied amphibolites with the chemical analysis of El-Rubshi amphibolites (El-Desoky et al., 2015). The studied samples were characterized by much higher contents of TiO_2, Al_2O_3, Fe_2O_3, MnO, Na_2O, LOI, Cr, Ni, Zn, Cu, Co, and V than El-Rubshi amphibolites. The studied amphibolite samples are distinguished by the abnormal contents of SiO_2 (38.4%), FeO (0.93%), MgO (8.26%), CaO (9.46%), Th (0.1%), Ba (36%), Zr (0.1%), Hf (0.23%), Ta (0.1%), and Nb (0.16%) compared to the El-Rubshi amphibolites. However, the amphibolite samples have low LOI contents (3.4 wt%), owing to their low alteration processes (**Table 1**). **Figure 12** shows the distribution of trace elements normalized to the primitive upper mantle (McDonough and Sun, 1995) for the amphibolite rocks in three areas: the present study, El-Rubshi area after El-Desoky et al. (2015), and Aegean, Greece after Stouraiti et al. (2017). All samples display a negative Zr-Cr–Ni anomaly and show relative enrichment in Th, Sr, and Cu.

The listwaenites are encountered in the Tilal Al-Qulieb and classified into two types: carbonate-rich listwaenite (17 and 18) and silica-carbonate rich listwaenite (45 and 46). The chemical analysis of the studied listwaenites compared to the chemical analysis of Wadi Garf listwaenites (El-Desoky and Saleh, 2012). From the geochemical point of view, it should be noted that carbonate-rich listwaenites are characterized by high concentrations of Al_2O_3, Fe_2O_3, MgO, CaO, Na_2O, Zn, and Co and low contents of SiO_2, TiO_2, FeO, MnO, P_2O_5, LOI, Cu, Pb, Ni, Sr, Ba, Zr, Nb, and Rb (**Table 2**).

The geochemical analysis of silica-rich listwaenites are characterized by high values of SiO_2, TiO_2, Al_2O_3, Fe_2O_3, Na_2O, K_2O, V, Ba, Zr, Y, and Rb (**Table 2**); meanwhile, the low values of FeO, MnO, MgO, CaO, P_2O_5, LOI, Cu, Pb, Zn, Ni, Co, Sr, Cr, and Nb are compared with Wadi Garf listwaenites (El-Desoky and Saleh, 2012). Sample number 46) silica-rich listwaenites exhibit deviation from the other samples. This sample was distinguished by high contents of SiO_2, Na_2O, K_2O, P_2O_5, Pb, U, Th, Ba, Zr, Sn, Y, Hf, Rb, Nb, Cs, and REEs compared to other samples (17, 18 and 45).

Geochemical analyses are consistent with expectations from petrography: carbonate listwaenite, which is remarkably high in SiO_2, Al_2O_3, and Fe_2O_3, at the expense of all other components. compared with the listwaenite of Jabal Ess, Saudi Arabia (Gahlan et al., 2020) while silica-carbonate listwaenite is similar in SiO_2 content compared with Gahlan et al., 2020 but high in Al_2O_3, Fe_2O_3, and CaO.

These rocks are affected by different alteration degrees of silicification and carbonization processes reinforced by petrographically studies and the contents of silica and loss-on-ignition (LOI) of these rocks, may reach high values (57.49% and 18.8 wt%, respectively, **Table 2**). Tilal Al-Qulieb talc carbonate rocks are characterized by high values of SiO_2, Al_2O_3, Fe_2O_3, MgO, LOI, Zn, Co, V, and Zr compared with El-Zarieb talc-carbonate rocks (Shaheen, 2012). Meanwhile, FeO, MnO, CaO, LOI, Pb, Ni, U, Th, Sr Cr, Ba, Y, Nb, Ta, Rb, and Ga exhibit low values (**Table 2**). The petrographically studies and loss-on-ignition (LOI; up to 46.4 wt%) contents of these rocks seem to be affected by carbonization alteration processes.

Figure 13C shows the normalized spider diagram of talc carbonate according to the primitive mantle. The comparison between three areas: the present study, El-Fawakhir after El-Shafei (2016) and Afghanistan after Tahir et al. (2018). All areas display a negative in most trace elements anomaly except La, Ce, Sr, and Zr.

Figure 13D shows the normalized spider diagram of listwaenites according to the primitive mantle. This diagram

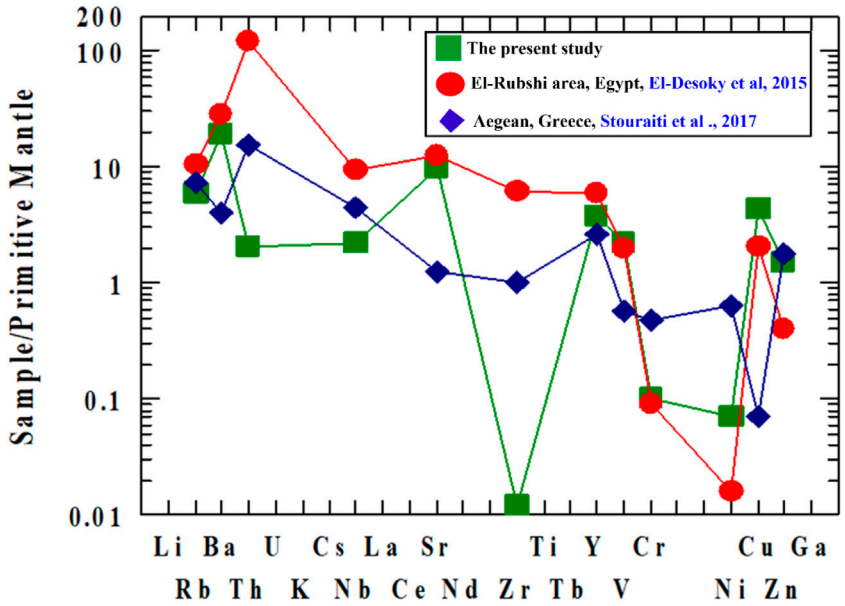

FIGURE 12 | PM-normalization values of average geochemical results of present amphibolite samples compared with El-Rubshi (Egypt) and Aegean (Greece) area.

shows the comparison between the present study and Gahlan et al. (2018) and the Sirsir area, Oman (Nasir et al., 2007). The basic trends of elements with simple differences in Nb, Zr, and Ni depletion are similar.

6.2 Mineralization

The mantle regions of ophiolites are excellent mining and exploration prospects. They are habitat to a wide range of ores (chromite, gold, and iron–nickel laterites) as well as industrial minerals (talc, asbestos, and serpentine) (Coleman, 1977; Klemm and Klemm, 2013; Gahlan et al., 2018 and Fu et al., 2019). Ophiolites and mineralization, including chromite, talc, asbestos, platinum-group elements, Cu–Ni–Co, magnesite, and gold, have a significant connection in the Eastern Desert (Klemm et al., 2001; Kusky and Ramadan, 2002; Azer et al., 2019). In the next sections, we will go through some of the most common resource kinds.

Listwaenite is an assemblage of carbonate minerals (magnesite, ankerite, and dolomite), quartz, and/or fuchsite (Cr-muscovite) together with disseminated sulfides and accessory minerals (Halls and Zhao, 1995). The term "listwaenite" is now commonly used by geologists for carbonated and/or silicified mafic-ultramafic rocks and will be used in the present work in this meaning. Listwaenite is regarded strictly to be a hydrothermal alteration product of mafic and ultramafic rocks (Buisson and Leblanc, 1987; Leblanc, 1991; El-Desoky and Saleh, 2012). Recently, listwaenite drew the attention of geologists because of its worldwide association with gold mineralization (Buisson and Leblanc, 1985; Buisson and Leblanc, 1986; Ash and Arksey, 1990; Aydal, 1990; Ucurum and Larson, 1999; Ucurum, 2000; El-Desoky and Saleh, 2012).

6.2.1 Ore Mineralogy of the Ophiolitic Rocks

This part aims to identify the most common opaque minerals hosted in the ophiolite ultramafics, with their alteration products in the studied district as well as the study of their textures, intergrowths, and distribution. To achieve this target, twelve polished slabs from the two areas were prepared. The samples were subjected to laboratory investigations like reflected light microscopy were taken showing the opaque minerals, textures, and their specific petrographic features.

Chromite, martite after magnetite, goethite, ilmenite, galena, and gold are the essential opaque minerals in the investigated area. The most prominent opaque mineral is chromite, whereas sulfides are in second place among the samples tested. Mineralization such as chromite, martite following magnetite, ilmenite, gold, and galena are deeply connected with Tilal Al-Qulieb ophiolitic rocks.

Chromite is shown as an anhedral to euhedral elongate, or even rectangular crystals, as well as zoned crystals of gray and reddish-brown (darker than magnetite) in color (**Figures 14A–C**). Takla (1982) demonstrated that rising serpentinization increases the amount of chromite zoning. In serpentinites, fractured chromite is found, but the cracks are filled by serpentine minerals (**Figures 14A–C**). It is constituted of huge chromite crystals that are bridged by serpentine, carbonate, talc, and chlorite veinlets. The grains are sometimes stained with yellowish or brownish iron oxyhydroxides materials. Galena is distinguished by either fine disseminations or small aggregates with sharp and irregular borders as well as bright white in color. It is usually three sets of cleavage, and moderately high reflectance is diagnostic (**Figure 14D**).

Magnetite occurs as euhedral to subhedral crystals of different sizes even in the same sample. Under reflected light, the mineral is

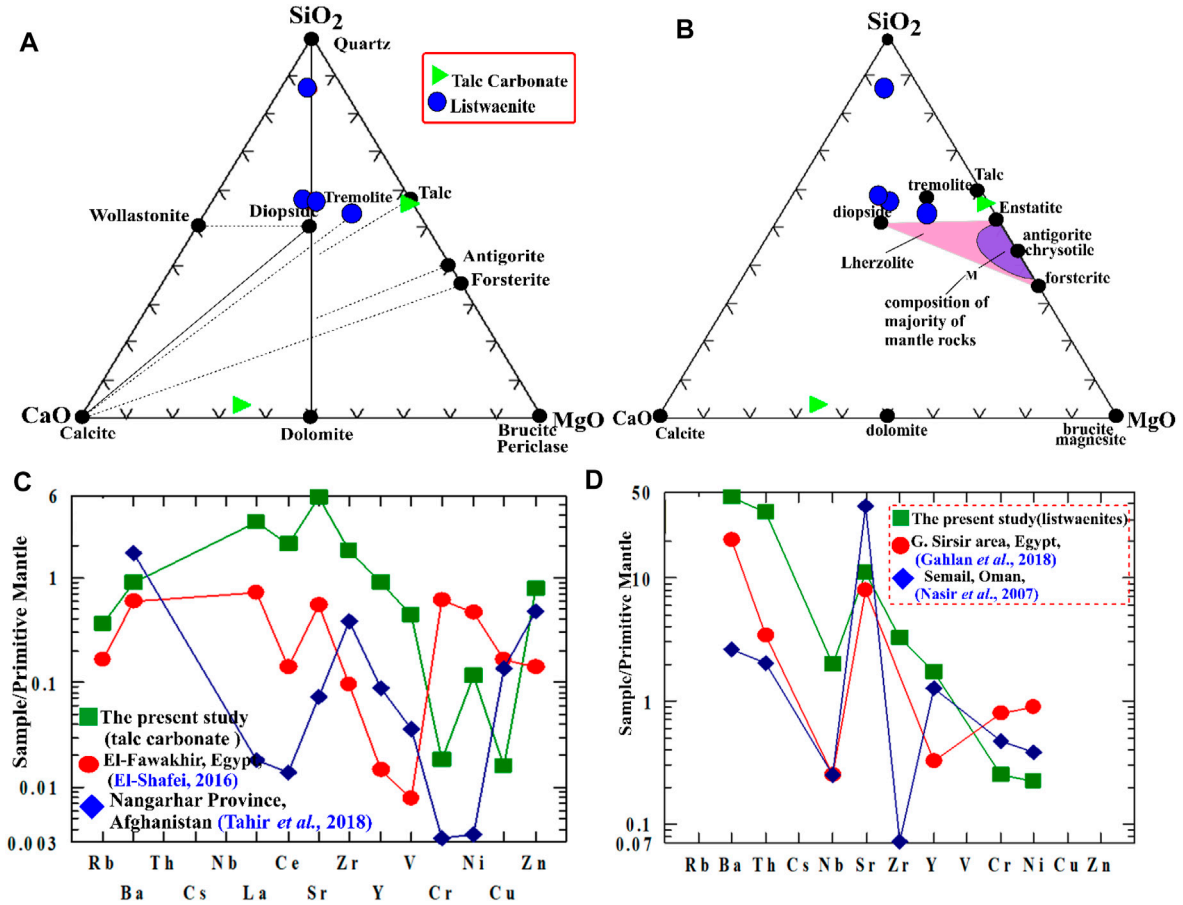

FIGURE 13 | (A) SiO_2–CaO–MgO diagram for listwaenites and talc-carbonate rocks (Bucher and Grapes, 2011). **(B)** SiO_2–CaO–MgO diagram for listwaenites and talc-carbonate rocks (Bucher and Grapes, 2011). **(C)** Primitive mantle-normalization results of the average geochemical of present samples of talc-carbonate compared with El-Fawakhir (Egypt) and Nangarhar province (Afghanistan). **(D)** Primitive mantle-normalization values of the average geochemical results of present listwaenite samples compared with Sirsir (Egypt) and Semail (Oman) area.

generally gray and completely replaced by hematite under oxidizing conditions. Magnetite is either slightly, strongly, or completely martitization. Martite is a later mineral that forms when the magnetite is oxidized to hematite pseudomorphs (**Figure 14E**). The hydrothermal activity of serpentine rocks is one of the main reasons for the formation of massive magnetite veins in the cracks (Gahlan and Arai, 2006 ; Hodel et al., 2017). Gold is found in listwaenites as little irregular single grains, specks, blebs, and fine disseminations. It happens when dispersed nuggets and quartz-carbonate coexist (**Figure 14F**). It has a bright yellow color with a greenish tint.

6.2.2 Alteration Mineralogy of the Host-Rocks (XRD)

From the perspective of this study, the detected minerals may be divided into two categories: ore minerals and related gangue alteration minerals. Ten samples from the Wadi Tilal Al-Qulieb area were analyzed by X-ray diffraction. The presence of ores such as chromite and magnetite is shown by X-ray diffraction of bulk ophiolite rocks (serpentinites and listwaenite) samples.

Antigorite, calcite, dolomite, quartz, bustamite, and ore deposits are found in the studied X-ray diffraction patterns of serpentinites (**Figures 15A, B**; magnetite and chromite). Antigorite is a high-temperature serpentine mineral, forming only above 250°C (Wenner and Taylor, 1974; Evans, 1977; Koutsovitis, 2017). Meanwhile, calcite, dolomite, tremolite, and graphite are used to make listwaenites (**Figures 15C, D**). Bustamite is a mineral that is found in carbonate-silicate-hosted deposits.

6.2.3 Chemistry of the Associated Ore Deposits (SEM)

Optical microscopy and XRD cannot study some of the trace phases since they are too tiny. Scanning electron microscopy (SEM) was used to examine twelve thin-polished slices, allowing for a thorough characterization of ore mineralogy and their interrelationships.

SEM images of ore minerals and their microchemical analyses are described as follows: within the Wadi Tilal Al-Qulieb serpentinites, ferromagnesiochromites ($FeMgCr_2O_4$) were discovered in abundance. Magnesiochromites have a significant amount of Fe^{+2} replacing Mg, and there is a constant Fe^{+2} > Mg fluctuation all the way down to the chromite itself (Deer et al., 1992). Ferromagnesiochromites are frequently seen as well-developed euhedral grains (**Figure 16**),

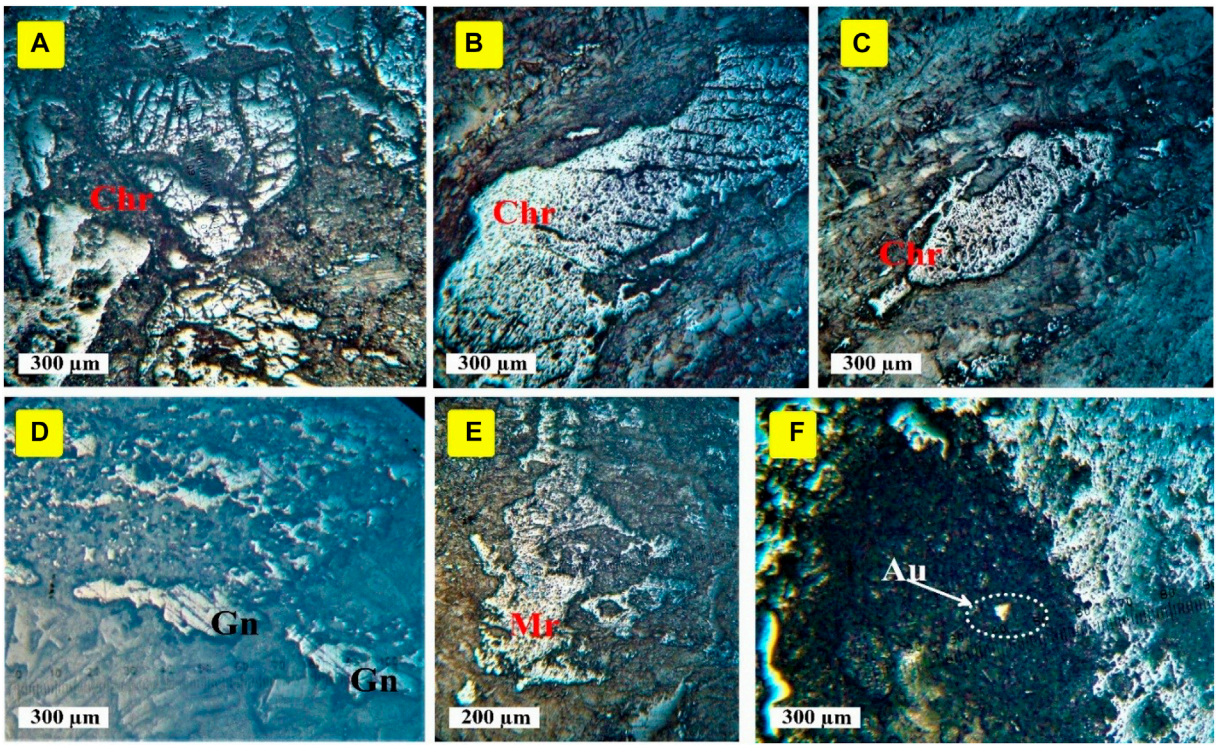

FIGURE 14 | Photomicrograph of the polished surface showing: **(A)** chromite, serpentinites, R. L. **(B)** Irregular fractured crystals of homogeneous chromite, serpentinites, R. L. **(C)** Chromite, serpentinites, R. L. **(D)** Fine-grained galena, serpentinites, R. L. **(E)** Magnetite grain completely altered to martite, serpentinites, R. L. **(F)** Gold nugget coexists with quartz-carbonate, listwaenite, R. L.

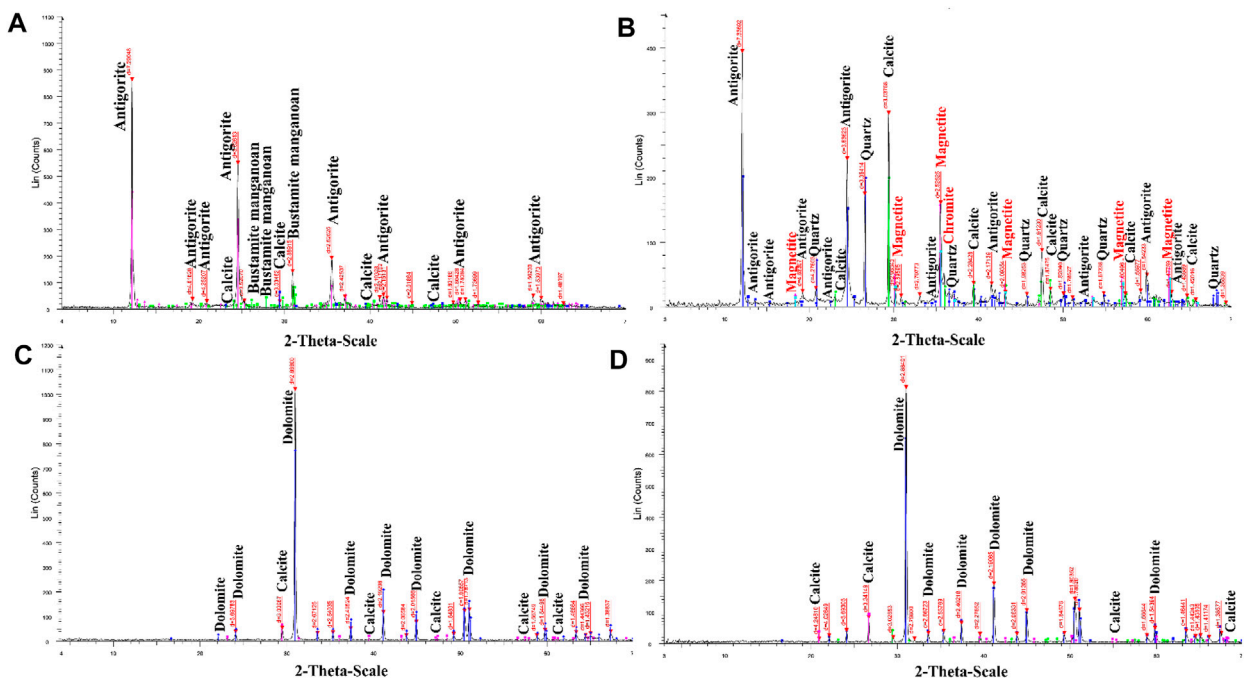

FIGURE 15 | X-ray diffraction patterns of the serpentinites showing **(A,B)** hydrothermal alterations: carbonization and serpentinization with chromite and magnetite ores. **(C,D)** X-ray diffraction patterns showing carbonization and silicification for the listwaenite studied samples.

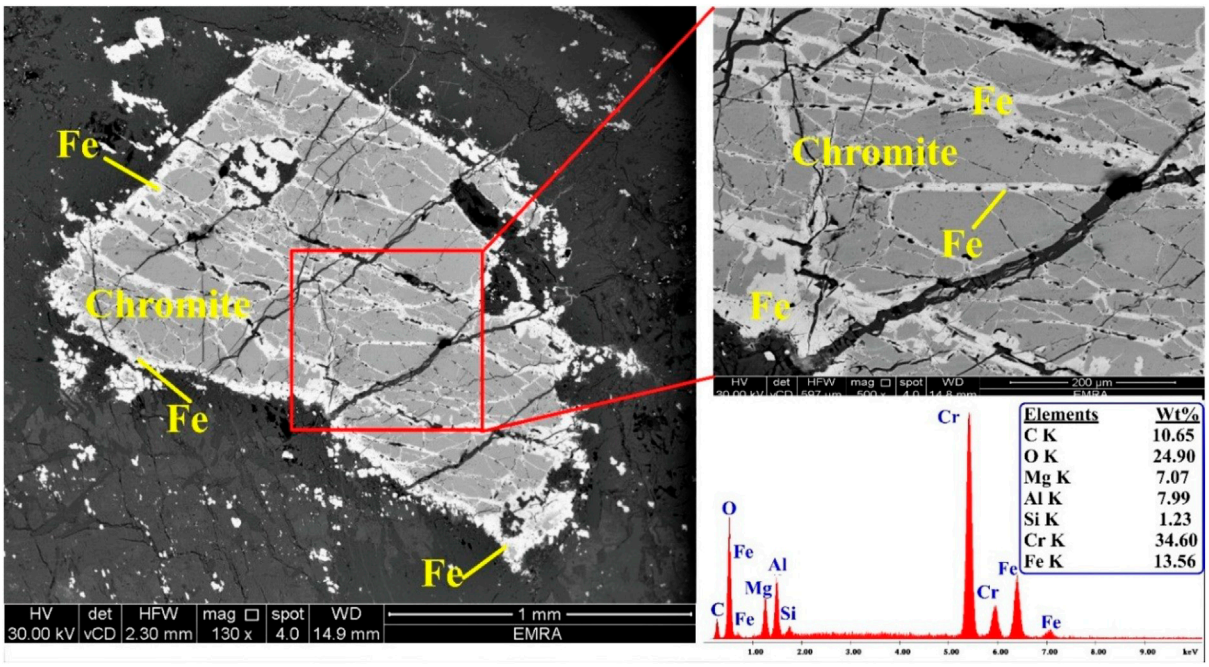

FIGURE 16 | SEM image of the euhedral crystal of Fe-Mg-chromite altered at the rim to iron oxide with sharp contact, serpentinite rocks.

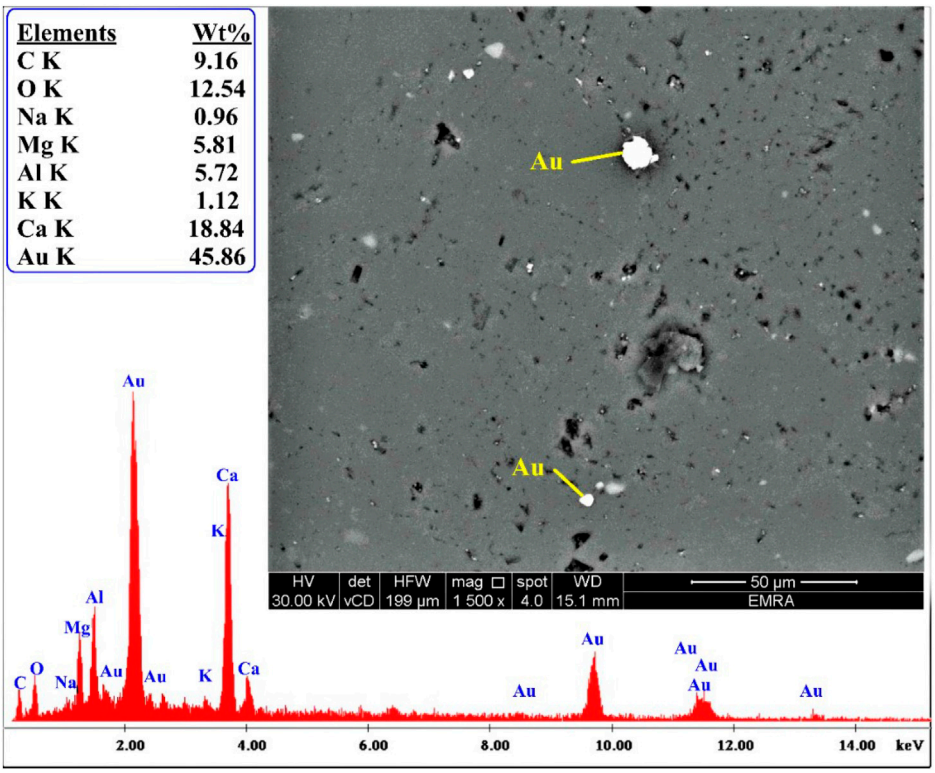

FIGURE 17 | SEM of gold nugget distributed in listwaenite rocks.

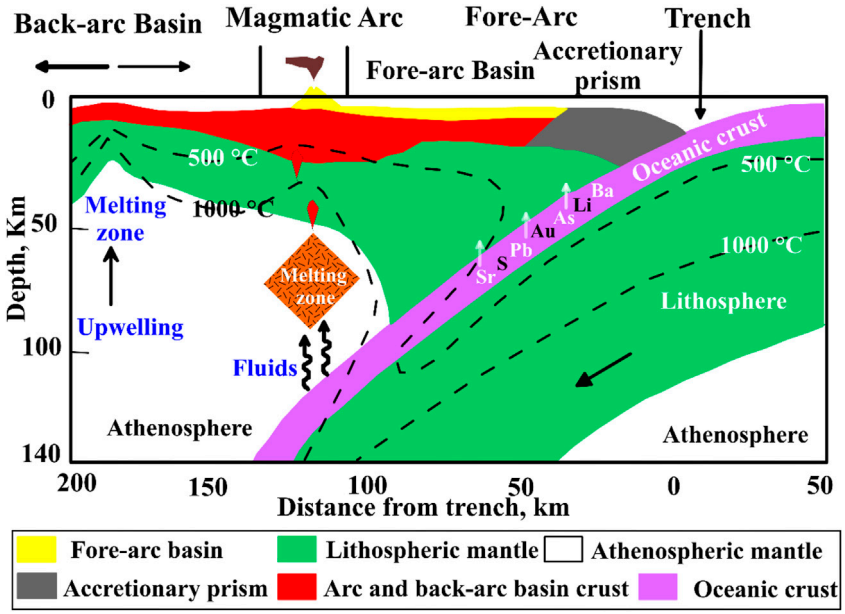

FIGURE 18 | Cartoon showing the tectonic setting of Tilal Al-Qulieb metasomatized peridotites in the fore-arc environment (modified after Azer and Stern 2007).

especially when they are linked with significant quantities of interstitial material. In the presence of chromite, the X-ray chart generated from EDX microchemical analysis shows strong peaks of chromium and iron indicator (**Figure 16**).

The chemical elemental composition of ferromagnesiochromites exhibits high values of chromium (31.75%–34.60%), iron (14.56%–18.79%), oxygen (24.90%–26.01%), and magnesium (7.07%–8.23%). Low levels of silicon (1.23%–1.91%) and carbon (6.51%–10.65%) were ascribed to contamination in the host rock (**Figure 16**). There is a significant amount of Cr replacement by Al (7.81%–7.99%), and significant amounts of Fe^{+3} may also replace Cr (Deer et al., 1992). As a result of iron oxidation or injection during metamorphism, iron microveinlets form within cracks infilling and along grain borders of chromite crystals (**Figure 16**). Because iron oxidation occurs in chromite, there is a vestige of Fe-chromite on the rim of chromite crystals (**Figure 16**). Thin laths are frequently used as replacements at grain borders or internal channel ways.

Gold is only recorded as disseminated nuggets in listwaenites at Tilal Al-Qulieb (**Figure 17**). It has a strongly bright color and seems to be epigenetic. Based on the microscopic studies, these gold grains could be formed as a result of hydrothermal fluids under mesothermal conditions. The EDX microchemical analysis of gold shows high Au (45.86%) content.

6.3 Alteration and Metamorphism

Alteration and metamorphism might have happened on the ocean bottom, underneath the oceanic crust, during and after tectonic emplacement, or after recent exposure. As a result, a range of sources and compositions for metamorphic fluids impacting ANS ophiolites have been hypothesized (Gahlan et al., 2018): i) CO_2-bearing fluids derived from the mantle (Boskabadi et al., 2017; Hamdy and El-Dien, 2017); ii) seawater at near-bottom temperatures (Snow and Dick 1995; Li and Lee 2006); iii) both H_2O-rich and CO_2-rich fluids released from various layers of a subducting slab (Bostock et al., 2002; Hamdy et al., 2013); and iv) hydrothermal fluids infiltrating during and after exhumation (˂100°C) (Seyfried and Dibble, 1980). The ophiolitic ultramafic rocks that outcrop in Egypt's SED are often heavily altered, although whether this alteration happened before, during, or after emplacement is frequently unknown. The ultramafic rocks are mostly transformed to serpentinite and/or serpentine-talc-carbonate composites (Abdel-Karim et al., 1996; Ghoneim et al., 1999; Ghoneim et al., 2003; El-Desoky et al., 2015). Serpentinites are metamorphic rocks that contain mostly serpentine minerals (lizardite, chrysotile, and/or antigorite), with brucite, magnetite, and Mg and Ca-Al silicates as minor phases (O'Hanley, 1996). Serpentinites are often black or green in color, with considerable levels of clay minerals present in yellowish to reddish rocks (Mével, 2003). Serpentinization is generated by the hydration of mafic or ultramafic rocks owing to action with fluids of diverse sources in a range of tectonic settings. In the oceans, serpentinites are mainly connected with downward fluid movement along with significant fault structures that reach deep into the lithosphere.

The most widespread types of ultramafic rock alteration are serpentinization and talc-carbonates. Only when the host rocks are mafic to ultramafic in composition do these kinds of alterations occur. These rocks have a greater iron and magnesium concentration than others. Serpentine is a low-temperature mineral, whereas the talc alteration suggests a greater magnesium content was present during crystallization.

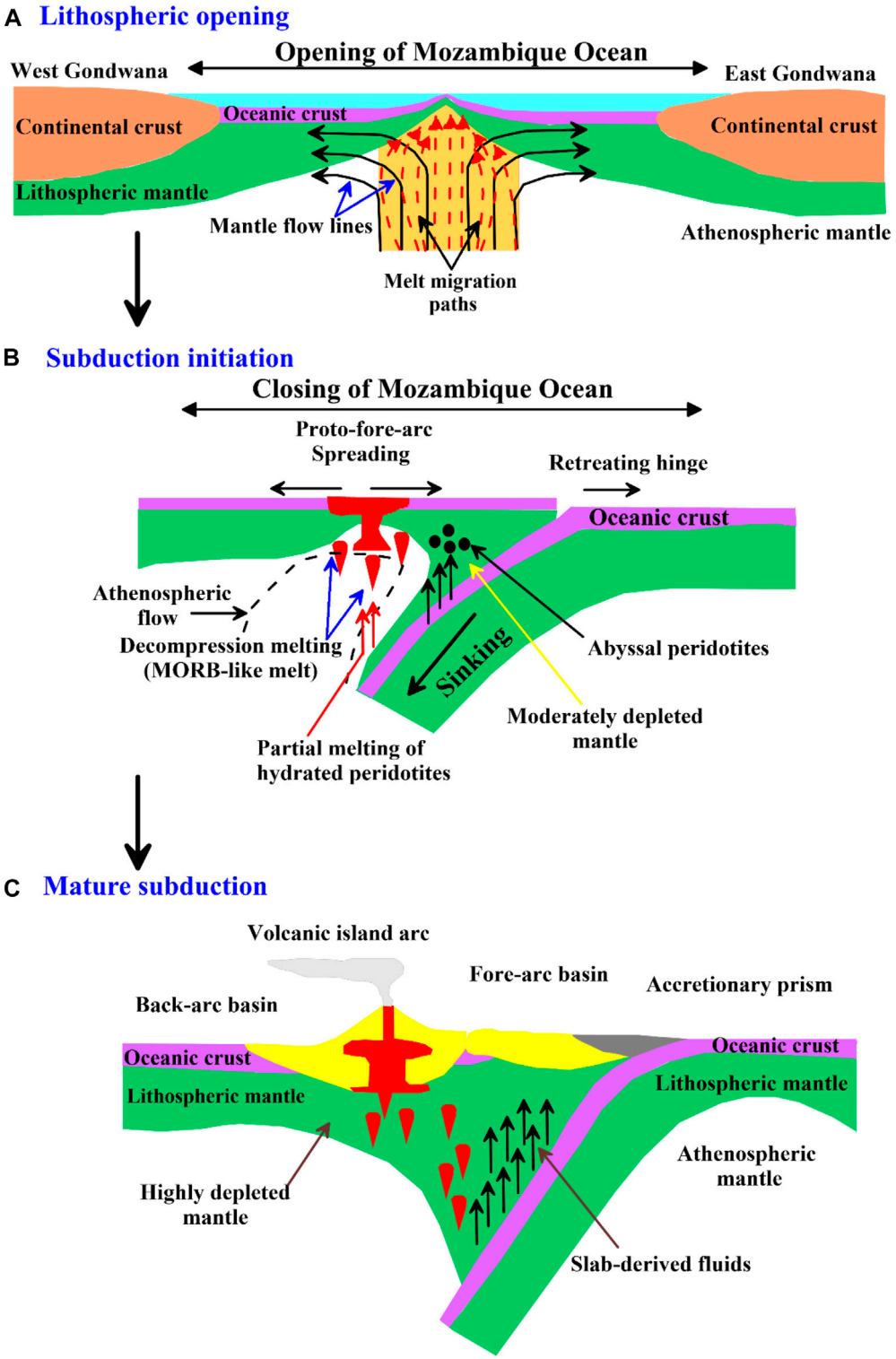

FIGURE 19 | Schematic illustration showing the tectonic model for the evolution of the studied ultramafic rocks and the Arabian–Nubian Shield. The carton was designed after a sketch by Whattam and Stern (2011), Moghadam et al. (2015), Khedr and Arai (2016), Gamal El Dien et al. (2016), and Abdel-Karim et al. (2021). **(A)** Opening of Mozambican ocean between East and West Gondwana; **(B)** subduction initiation or incipient arc stage, in which partial melting occurred in the mantle wedge and the proto-forearc spreading starts to form over the subduction zone; the serpentinites and pyroxenites of Wadi Al-Qulieb were formed in this stage; and **(C)** development of mature subduction or a mature-arc stage which is associated with tremendous slab-derived fluids and highly partial melting of depleted mantle produces peridotite serpentinite melts.

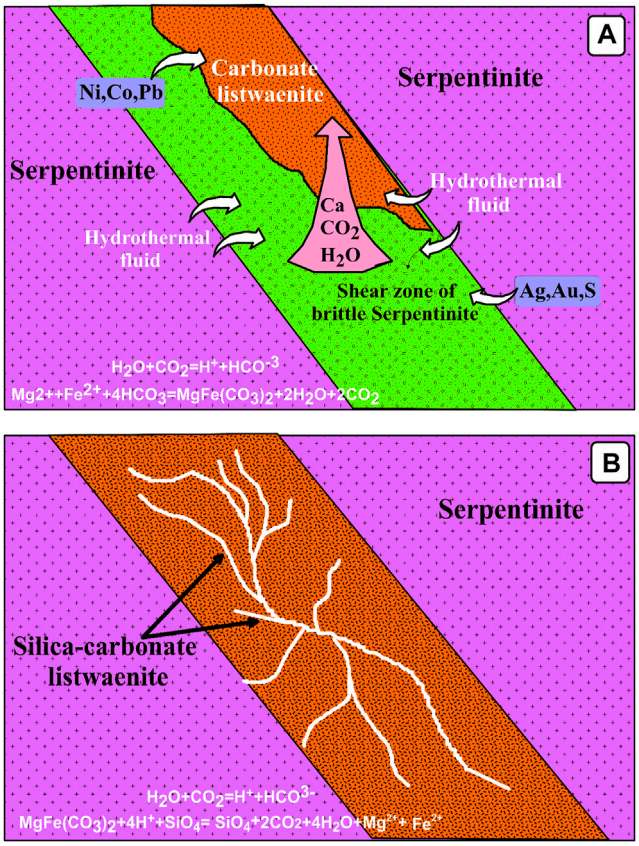

FIGURE 20 | Cartoon for an idealized petrogenetic model of listwaenites (after Ucurum et al., 1996) in the wadi Allaqi, Southeastern Desert of Egypt, based on field observations, petrography, and geochemistry. **(A)** Serpentinite protolith breaks down and is changed to carbonate-rich listwaenite form as CO_2-rich hydrothermal fluids infiltrate through and precipitate Mg-Fe-Ca carbonates in its place. Gold is released into a solution associated with sulfide. **(B)** Silica-rich listwanites form because the hydrothermal fluids are protected from the serpentinite by the precipitation of carbonates in the initial phase of alteration. As a result, fluids become increasingly acidic, encouraging carbonate breakdown and the precipitation of silica, sulfides, and gold.

During alteration, LOI was employed to track the amount of element redistribution (Polat and Hofmann, 2003). The greater LOI concentrations in serpentinites from the examined locations indicate that the parent rocks are more hydrated.

Carbonation is shown in serpentinites, listwaenites, and talc carbonates. Carbonation occurs when CO_2–rich fluids interact with sensitive rocks in the crust and mantle, resulting in the alteration and formation of carbonate along faults as well as shear zones (Pirajno, 2009 and; Azer, 2013). Seawater alteration and regional metamorphism are both responsible for carbonate changes in the greenstone belts. Serpentine minerals predate the creation of carbonates in several greenstone belts, and stable-isotope data show that serpentinization was caused by saltwater or a hydrothermal fluid resulting from fluid-rock interaction (Kyser and Kerrich, 1991; O'Hanley et al., 1993).

At Wadi Tilal Al-Qulieb, chromite rims have been converted to Cr-magnetite. Several writers, including Takla et al. (1975) and Ghoneim and Szederkeny (1979) have described the transformation of chromite to such highly reflective rims result of regional metamorphism. The chromite lenses have a disparity and a high degree of alteration.

6.4 Geodynamic Evolution of the Neoproterozoic Mantle

According to the aforementioned findings, the metasomatized peridotite serpentinites of Tilal Al-Qulieb are similar to most Egyptian ophiolites' hypothesized tectonic settings, which included oceanic lithosphere pieces emplaced over a subduction zone in a forearc setting (**Figure 18**; e.g., Azer and Stern 2007; Hamdy and Lebda 2011; Azer et al., 2013; Abdel-Karim et al., 2014). The metasomatized peridotites of Tilal Al-Qulieb, on the other hand, have unique whole-rock chemical compositions, implying that they formed in several phases:

First phase: Peridotites were formed in the initial stage of the Mozambican Ocean's opening between East and West Gondwana, as relics of MOR-type melting under the midocean ridge system (**Figure 19A**).

Second phase: As a result of the closing of the Mozambican Ocean during the subduction initiation stage (Jöns and Schenk 2007), originally developed abyssal peridotites were subsequently emplaced in the subduction zone (**Figure 19B**). The resemblance of Tilal Al-Qulieb samples to abyssal peridotites, on the other hand, indicates that these rocks might have formed at a proto-forearc spreading center during the subduction initiation stage (Khedr and Arai 2016).

Third Phase: In the final phases, we believe that the studied ultramafic most refractory peridotites evolved at a mature arc stage as a result of high-degree partial melting of the sub-forearc mantle (**Figure 19C**).

All the silica-carbonate, and some carbonate listwaenites in the study area formed along the major and minor thrust faults inside or bordering serpentinized ultramafic rocks. Formation models for the listwaenites bodies at wadi Tilal Al-Qulieb, based primarily on alteration assemblages and element associations, are summarized in **Figure 20**.

All the silica-carbonate, and some carbonate listwaenites in the study area formed along the major and minor thrust faults inside or bordering serpentinized ultramafic rocks. Thrust fault zones acted as pathways for hydrothermal fluids (**Figure 20A**). In carbonate listwaenites, the mineralizing fluids are considered to pass through a porous and weak (including several small-scale cracks and faults) and highly altered serpentinite zone (**Figure 20B**).

7 CONCLUSION

Dismembered ultramafic rocks were encountered in the Tilal Al-Qulieb area, Southeastern Desert, Egypt. Serpentines, talc-carbonate rocks, listwaenite, and amphibolites, as well as small outcrops of pyroxenite are among the exposed ultramafic rocks in the field of study. Serpentinites are composed of more than 90% serpentine minerals (antigorite and crysotile) with minor

carbonate, opaque minerals, and talc. The appearance of antigorite in serpentinites indicates that low-grade metamorphism has begun (greenschist facies). Hydrothermal alteration types of serpentinites range from talc-carbonate rocks to listwaenites. Ophiolitic rock alteration is frequently caused by interaction with migrating carbonate-rich fluids. The petrogenesis of the serpentinites revealed that these rocks were formed after lherzolite–peridotite and tectonically represent a transitional phase between abyssal and subduction zone-related serpentinites, and at the beginning of subduction, the abyssal serpentinites (especially dehydrated orogenic peridotite) were thrusted or obducted forming the present ophiolitic serpentinites and the associated subduction-related metasediments. The information given here shows that Wadi Allaqi mantle peridotites are equivalent to the supra-subduction zone fore-arc origin. The amphibolites were derived from metamorphosed basic rocks of tholeiitic nature. The listwaenite and talc-carbonate rocks revealed that they trend toward silica, carbonate, and talc. Listwaenite is classified into two types: carbonate-rich listwaenite and silica–carbonate-rich listwaenite. The opaque minerals were examined by reflecting microscopy, XRD, and SEM techniques. They are hosted in the ophiolite ultramafic rocks including chromite, magnetite, martite, galena, and gold. The degree of alteration determines the production of ferrochrome, which is often generated during low to medium-grade metamorphism. These rocks are affected by different alteration degrees of serpentinization, silicification, and carbonization processes reinforced by petrographical studies and the contents of silica and loss-on-ignition (LOI) of these rocks. Compatible elements such as Ni, Cu, V, Co, and Cr are abundant in ultramafic rocks (serpentinites, amphibolites, and quartz-carbonate rocks). Carbonate veinlets encountered in the host rocks are composed of dolomite and calcite.

DATA AVAILABILITY STATEMENT

The raw data supporting the conclusion of this article will be made available by the authors, without undue reservation.

AUTHOR CONTRIBUTIONS

Conceptualization, HE-D, HZ, and HA; methodology, BS and HE-A; software, AA-R and WF; validation, HE-A and MH;formal analysis, HZ, AT, and AA-R; investigation, WF; resources, AE, HE-D, and ST; data curation, BS, and MH; writing—"original draft preparation, HE-D, BS, and AA-R; writing—"review and editing, HZ, ST, AE, and MH; visualization,WF, HA, and HE-A; supervision, AE and HE-A; project administration, HZ and HE-A; All authors have read and agreed to the published version of the manuscript.

ACKNOWLEDGMENTS

The authors thank the "Dunarea de Jos" University of Galati, Romania, for the APC support. The researcher (HA) is funded by a scholarship under the Joint (Executive Program between Egypt and Russia).

REFERENCES

Abd El-Naby, H. H., and Frisch, W. (2002). Origin of the Wadi Haimur-Abu Swayel Gneiss Belt, South Eastern Desert, Egypt: Petrological and Geochronological Constraints. *Precambrian Res.* 113, 307–322. doi:10.1016/s0301-9268(01)00214-5

Abdel-Karim, A.-A. M., Ali, S., and El-Shafei, S. A. (2018). Mineral Chemistry and Geochemistry of Ophiolitic Metaultramafics from Um Halham and Fawakhir, Central Eastern Desert, Egypt. *Int. J. Earth Sci. Geol. Rundsch)* 107 (7), 2337–2355. þ. doi:10.1007/s00531-018-1601-2

Abdel-Karim, A.-A. M., Ali, S., Helmy, H. M., and El-Shafei, S. A. (2016). A Fore-Arc Setting of the Gerf Ophiolite, Eastern Desert, Egypt: Evidence from Mineral Chemistry and Geochemistry of Ultramafites. *Lithos* 263, 52–65. þ. doi:10.1016/j.lithos.2016.05.023

Abdel-Karim, A.-A. M., El-Shafei, S. A., and Azer, M. K. (2021). The Neoproterozoic Ophiolitic Ultramafic Rocks in Eastern Desert of Egypt: Implications for Petrogenesis and Metasomatic Processes. *Int. Geol. Rev.* 63 (2), 208–232. þ. doi:10.1080/00206814.2019.1708816

Abdel-Karim, A.-A. M., Elwan, W. I., Helmy, H., and El-Shafey, S. A. (2014). Spinels, Fe-Ti Oxide Minerals, Apatites and Carbonates Hosted in the Ophiolites of Eastern Desert of Egypt: Mineralogy and Chemical Aspects. *Arab. J. Geosci.* 7 (2), 693–709. doi:10.1007/s12517-013-0854-0

Abdel-Karim, A. M., El-Mahallawi, M. M., and Finger, F. (1996). The Ophiolite Mélange of Wadi Dungash and Arayis, Eastern Desert of Egypt: Petrogenesis and Tectonic Evolution. *Acta Mineral. Petrogr. Szeged* 37, 129–141. http://digit.bibl.uszeged.hu/00100/00156/00049/mineralogica_037.pdf#page=130.

Abdelsalam, M. G., Abdeen, M. M., Dowaidar, H. M., Stern, R. J., and Abdelghaffar, A. A. (2003). Structural Evolution of the Neoproterozoic Western Allaqi-Heiani Suture, Southeastern Egypt. *Precambrian Res.* 124, 87–104. doi:10.1016/s0301-9268(03)00080-9

Abdelsalam, M. G., and Stern, R. J. (1996). Sutures and Shear Zones in the Arabian-Nubian Shield. *J. Afr. Earth Sci.* 23, 289–310. doi:10.1016/s0899-5362(97)00003-1

Abu El-Ela, F. F. (1996). The Petrology of the Abu Zawal Gabbroic Intrusion, Eastern Desert, Egypt: an Example of an Island-Arc Setting. *J. Afr. Earth Sci.* 22 (2), 147–157. doi:10.1016/0899-5362(96)00004-8

Ahmed, A. H., and Habtoor, A. (2015). Heterogeneously Depleted Precambrian Lithosphere Deduced from Mantle Peridotites and Associated Chromitite Deposits of Al'Ays Ophiolite, Northwestern Arabian Shield, Saudi Arabia. *Ore Geol. Rev.* 67, 279–296. doi:10.1016/j.oregeorev.2014.12.018

Akaad, M. K., and Noweir, A. M. (1980). Geology and Lithostratigraphy of the Arabian Desert Orogenic Belt of Egypt between Lat. 25°35′ and 26°30′N. *Bull. Inst. Appl. Geol.* 3 (4), 127–135. King Abdul Aziz Univ., Jeddah.

Ali, K. A., Azer, M. K., Gahlan, H. A., Wilde, S. A., Samuel, M. D., and Stern, R. J. (2010). Age Constraints on the Formation and Emplacement of Neoproterozoic Ophiolites along the Allaqi-Heiani Suture, South Eastern Desert of Egypt. *Gondwana Res.* 18, 583–595. doi:10.1016/j.gr.2010.03.002

Ash, C. H., and Arksey, R. L. (1990).The Atlin Ultramafic Allochthon: Ophiolite Basement within the Cache Creek Terranes; Tectonic and Metallogenic Significance: (104N/12). *Geol. Fieldwork* 1989þ, 1990–1991.

Awad, H. A., Abu El-Leil, I., El-wardany, R., Ene, A., Tolba, A., Kamel, M., et al. (2022a). Mineralogy and Radioactivity Level of the New Occurrence of Ilmenite Bearing Gabbro at Abu Murrat, Northeastern Desert, Egypt. *Rom. J. Phys.* 67 (3-4), 803. Available at: https://www.researchgate.net/publication/358397203_Mineralogy_and_Radioactivity_Level_of_the_New_Occurrence_of_Ilmenite_

Bearing_Gabbro_at_Abu_Murrat_Northeastern_Desert_Egypt (Accessed April 28, 2022).

Awad, H. A., Abu El-Leil, I., Nastavkin, A. V., Tolba, A., Kamel, M., El-Wardany, R. M., et al. (2022b). Statistical Analysis on the Radiological Assessment and Geochemical Studies of Granite Rocks in the North of Um Taghir Area, Eastern Desert, Egypt. *Open Chem.* 20, 254–266. doi:10.1515/CHEM-2022-0131/MACHINEREADABLECITATION/RIS

Awad, H. A., Zakaly, H. M. H., Nastavkin, A. V., El Tohamy, A. M., and El-Taher, A. (2021). Radioactive Mineralizations on Granitic Rocks and Silica Veins on Shear Zone of El-Missikat Area, Central Eastern Desert, Egypt. *Appl. Radiat. Isotopes* 168, 109493. doi:10.1016/j.apradiso.2020.109493

Aydal, D. (1990). Gold-bearing Listwaenites in the Araç Massif, Kastamonu, Turkey. *Terra nova.* 2 (1), 43–52. doi:10.1111/j.1365-3121.1990.tb00035.x

Azer, M. K. (2013). Evolution and Economic Significance of Listwaenites Associated with Neoproterozoic Ophiolites in South Eastern Desert, Egypt. *Geol. Acta* 11 (1), 113–128. https://revistes.ub.edu/index.php/GEOACTA/article/view/105.000001777.

Azer, M. K., Gahlan, H. A., Asimow, P. D., Mubarak, H. S., and Al-Kahtany, K. M. (2019). Multiple Stages of Carbonation and Element Redistribution during Formation of Ultramafic-Hosted Magnesite in Neoproterozoic Ophiolites of the Arabian-Nubian Shield, Egypt. *J. Geol.* 127, 81–107. doi:10.1086/700652

Azer, M. K., and Khalil, A. E. S. (2005). Petrological and Mineralogical Studies of Pan-African Serpentinites at Bir Al-Edeid Area, Central Eastern Desert, Egypt. *J. Afr. Earth Sci.* 43, 525–536. doi:10.1016/j.jafrearsci.2005.09.008

Azer, M. K., Samuel, M. D., Ali, K. A., Gahlan, H. A., Stern, R. J., Ren, M., et al. (2013). Neoproterozoic Ophiolitic Peridotites along the Allaqi-Heiani Suture, South Eastern Desert, Egypt. *Min. Pet.* 107 (5), 829–848. doi:10.1007/s00710-012-0204-z

Azer, M. K., and Stern, R. J. (2007). Neoproterozoic (835–720 Ma) Serpentinites in the Eastern Desert, Egypt: Fragments of Forearc Mantle. *J. Geol.* 115, 457–472. doi:10.1086/518052

Bodinier, J.-L., and Godard, M. (2014). "Orogenic, Ophiolitic, and Abyssal Peridotites," in *Mantle and Core. Treatise on Geochemistry*. Editor R. W. Carlson (Elsevier Science Ltd.), 2, 103–167. doi:10.1016/B978-0-08-095975-7.00204-7

Boskabadi, A., Pitcairn, I. K., Broman, C., Boyce, A., Teagle, D. A. H., Cooper, M. J., et al. (2017). Carbonate Alteration of Ophiolitic Rocks in the Arabian–Nubian Shield of Egypt: Sources and Compositions of the Carbonating Fluid and Implications for the Formation of Au Deposits. *Int. Geol. Rev.* 59 (4), 391–419. doi:10.1080/00206814.2016.1227281

Bostock, M. G., Hyndman, R. D., Rondenay, S., and Peacock, S. M. (2002). An Inverted Continental Moho and Serpentinization of the Forearc Mantle. *Nature* 417 (6888), 536–538. doi:10.1038/417536a

Botros, N. S. (2004). A New Classification of the Gold Deposits of Egypt. *Ore Geol. Rev.* 25, 1–37. doi:10.1016/j.oregeorev.2003.07.002

Bucher, K., and Grapes, R. (2011). *Petrogenesis of Metamorphic Rocks*, 345p. Springer, New York. doi:10.1007/978-3-540-74169-5

Buisson, G., and Leblanc, M. (1985). Gold in Carbonatized Ultramafic Rocks from Ophiolite Complexes. *Econ. Geol.* 80 (7), 2028–2029. þ. doi:10.2113/gsecongeo.80.7.2028

Buisson, G., and Leblanc, M. (1987). Gold in Mantle Peridotites from Upper Proterozoic Ophiolites in Arabia, Mali, and Morocco. *Econ. Geol.* 82, 2091–2097. doi:10.2113/gsecongeo.82.8.2091

Buisson, G., and Leblanc, M. (1986). Gold-bearing Listwaenites (Carbonatized Ultramafic Rocks) from Ophiolite Complexes. In Conference metallogeny of basic and ultrabasic rocks United Kingdom: IMM Publication (pp. 121–131).þ http://pascal-francis.inist.fr/vibad/index.php?action=getRecordDetail&idt=8819801.

Coleman, R. G., and Keith, T. E. (1971). A Chemical Study of Serpentinization--Burro Mountain, California. *J. Petrology* 12 (2), 311–328. doi:10.1093/petrology/12.2.311

Coleman, R. G. (1977). *Ophiolites-Ancient Oceanic Lithosphere*. New York, Berlin: Springer-Verlag. doi:10.1180/minmag.1978.042.322.42

Deer, W. A., Howie, R. A., and Zussman, J. (1992). *An Introduction to the Rock-Forming Minerals*. 2nd ed. England: Longman, 696. doi:10.1180/minmag.1992.056.385.20

Deschamps, F., Godard, M., Guillot, S., and Hattori, K. (2013). Geochemistry of Subduction Zone Serpentinites: A Review. *Lithos* 178, 96–127. doi:10.1016/j.lithos.2013.05.019

Dilek, Y., Furnes, H., and Shallo, M. (2008). Geochemistry of the Jurassic Mirdita Ophiolite (Albania) and the MORB to SSZ Evolution of a Marginal Basin Oceanic Crust. *Lithos* 100 (1-4), 174–209. doi:10.1016/j.lithos.2007.06.026

Dilek, Y., and Newcomb, S. (2003). Ophiolite Concept and the Evolution of Geological Thought. *Geol. Soc. Amer Spec. Pap.* 373, 504. doi:10.1017/S0016756804239437

Dixon, T. H. (1979). *Evolution of Continental Crust in the Late Precambrian Egyptian Shield*. San Diego: Thesis, University of California. https://www.osti.gov/biblio/5413925.

El-Bahariya, G. A. (2021). Ghadir Ophiolites, Eastern Desert, Egypt: A Complete Sequence of Oceanic Crust in the Arabian-Nubian Shield. In *The Geology of the Arabian-Nubian Shield* (pp. 331–342). Springer, Cham.þ doi:10.1007/978-3-030-72995-0_13

El-Bahariya, G. A. (2019).*Geochemistry and Tectonic Setting of Neoproterozoic Rocks from the Arabian-Nubian Shield: Emphasis on the Eastern Desert of Egypt*. Eastern Desert of Egypt: Intec Open. doi:10.5772/intechopen.825191-25

El-Desoky, H. M., and Khalil, A. E. (2011). Evolution of the Talc-Carbonate Rocks in Umm Rilan Ophiolite, South Eastern Desert, Egypt: Implication from Mineralogy, Petrography, Geochemistry and P-T Conditions. *Al-Azhar Bull. Sci.*, 22 (2), 1–32. doi:10.21608/absb.2011.7908

El-Desoky, H. M., Khalil, A. E., and Salem, A. K. A. (2015). Ultramafic Rocks in Gabal El-Rubshi, Central Eastern Desert, Egypt: Petrography, Mineral Chemistry, and Geochemistry Constraints. *Arab. J. Geosci.* 8 (5), 2607–2631. doi:10.1007/s12517-014-1407-x

El-Desoky, H. M., and Saleh, G. M. (2012). Petrological, Mineralogical and Geochemical Characterization of Listwaenite from the Late Proterozoic Wadi Garf Ophiolite, South Eastern Desert, Egypt: An Implication for Mobility of Elements during Listwaenitization. *Egypt. J. Geol.* 56, 433–456. doi:10.1016/J.CHEMER.2005.01.003

El-Ramly, M. F. (1972). A New Geological Map for the Basement Rocks in the Eastern and Southwestern Deserts of Egypt. *Ann. Geol. Surv. Egypt* 2, 1–18.

El-Sayed, M. M., Furnes, H., and Mohamed, F. H. (1999). Geochemical Constraints on the Tectonomagmatic Evolution of the Late Precambrian Fawakhir Ophiolite, Central Eastern Desert, Egypt. *J. Afr. Earth Sci.* 29, 515–533. doi:10.1016/s0899-5362(99)00113-x

El-Shafei, S. H. (2016). *Mantle Peridotites Host Listwaenites of Some Proterozoic Ophiolites in Eastern Desert of Egypt and Their Relationship with Gold Deposits* (Zagazig University). PHD Thesis.

Evans, B. W. (1977). Metamorphism of Alpine Peridotite and Serpentinite. *Annu. Rev. Earth Planet. Sci.* 5 (1), 397–447. doi:10.1146/annurev.ea.05.050177.002145

Gahlan, H. A., and Arai, S. (2006). Genesis of Peculiarly Zoned Co, Zn and Mn-Rich Chromian Spinel in Serpentinite of Bou-Azzer Ophiolite, Anti-atlas, Morocco. *J. Mineralogical Petrological Sci.* 102 (3), 216. doi:10.2465/JMPS.060212

Gahlan, H. A., Azer, M. K., Asimow, P. D., and Al-Kahtany, K. M. (2020). Petrogenesis of Gold-Bearing Listvenites from the Carbonatized Mantle Section of the Neoproterozoic Ess Ophiolite, Western Arabian Shield, Saudi Arabia. *Lithos* 372-373, 105679. doi:10.1016/j.lithos.2020.105679

Gahlan, H. A., Azer, M. K., and Asimow, P. D. (2018). On the Relative Timing of Listwaenite Formation and Chromian Spinel Equilibration in Serpentinites. *Am. Mineralogist J. Earth Planet. Mater.* 103 (7), 1087–1102. doi:10.2138/am-2018-6473

Gamal El Dien, H., Hamdy, M., Abu El-Ela, A. S., Abu-Alam, T., Hassan, A., Kil, Y., et al. (2016). Neoproterozoic Serpentinites from the Eastern Desert of Egypt: Insights into Neoproterozoic Mantle Geodynamics and Processes beneath the Arabian–Nubian Shield. *Precambrian Res.* 286, 213–233. doi:10.1016/j.precamres.2016.10.006

Ghoneim, M. F., Salem, I. A., and Hamdy, M. M. (1999). On the Petrogenesis of Magnesite from Gebel El-Maiyit, Central Eastern Desert, Egypt. *GAW4, Int. Conf. Geol. Arab World, Cairo Univ., Egypt* 1, 575–593.

Ghoneim, M. F., Salem, I. A., and Hamdy, M. M. (2003). Origin of Magnesite Veins in Serpentinites from Mount El-Rubshi and Mount El-Maiyit, Eastern Desert,

Egypt. *Arch. Mineral.* 54, 41–63. https://www.researchgate.net/publication/255451137.

Ghoneim, M., and Szederkeny, T. (1979). Petrological Review of the Ofalu Serpentinite; Mecsek Mountains, Hungary. *Acta Petrogr. Szeged* 24 (1), 5–18. doi:10.1016/0013-4686(79)87042-5

Greiling, R. O., Abdeen, M. M., Dardir, A. A., El Akhal, H., El Ramly, M. F., El Din Kamal, G. M., et al. (1994). A Structural Synthesis of the Proterozoic Arabian-Nubian Shield in Egypt. *Geol. Rundsch* 83 (3), 484–501. þ. doi:10.1007/bf01083222

Gülaçar, O. F., and Delaloye, M. (1976). Geochemistry of Nickel, Cobalt and Copper in Alpine-type Ultramafic Rocks. *Chem. Geol.* 17, 269–280. doi:10.1016/0009-2541(76)90041-3

Halls, C., and Zhao, R. (1995). Listwaenite and Related Rocks: Perspectives on Terminology and Mineralogy with Reference to an Occurrence at Cregganbaun, Co. Mayo, Republic of Ireland. *Miner. Deposita* 30 (3), 303–313. doi:10.1007/bf00196366

Hamdy, M. M., and El-Dien, H. M. G. (2017). Nature of Serpentinization and Carbonation of Ophiolitic Peridotites (Eastern Desert, Egypt): Constrains from Stable Isotopes and Whole-Rock Geochemistry. *Arabian J. Geosciences* 10 (19), 1–17. doi:10.1007/s12517-017-3215-6

Hamdy, M. M., Harraz, H. Z., and Aly, G. A. (2013). Pan-African (Intraplate and Subduction-Related?) Metasomatism in the Fawakhir Ophiolitic Serpentinites, Central Eastern Desert of Egypt: Mineralogical and Geochemical Evidences. *Arab. J. Geosci.* 6 (1), 13–33. doi:10.1007/s12517-011-0319-2

Hamdy, M. M., and Lebda, E. M. M. (2011). Al-compositional Variation in Ophiolitic Chromitites from the South Eastern Desert of Egypt: Petrogenetic Implications. *J. Geol. Min. Res.* 3 (9), 232–250. doi:10.1130/B30446.1

Heier, K. S. (1960). Petrology and Geochemistry of High Grade Metamorphic and Igneous Rocks on Langøy, Northern Norway. *J', Org. Geol. Unders.* 207, 1–246. doi:10.1016/0016-7037(71)90106-2

Hodel, F., Macouin, M., Triantafyllou, A., Carlut, J., Berger, J., Rousse, S., et al. (2017). Unusual Massive Magnetite Veins and Highly Altered Cr-Spinels as Relics of a Cl-Rich Acidic Hydrothermal Event in Neoproterozoic Serpentinites (Bou Azzer Ophiolite, Anti-atlas, Morocco). *Precambrian Res.* 300, 151–167. doi:10.1016/j.precamres.2017.08.005

Ishii, T., Robinson, P. T., Maekawa, H., and Fiske, R. (1992). "Petrological Studies of Peridotites from Diapiric Serpentinite Seamounts in the Izu- Ogasawara-Mariana Forearc, Leg 125," in *Proceedings of the Ocean Drilling Project, Leg 125, Scientific Results*. Editors J. A. Pearce L. B. Stokking, et al. (Scientific Results publishing: College Station, TX), 445–485. doi:10.2973/odp.proc.sr.125.129.1992

Jagoutz, E., Palme, H., Baddenhausen, H., Blum, K., Cendales, M., Dreibus, G., et al. (1979). The Abundances of Major, Minor and Trace Elements in the Earth's Mantle as Derived from Primitive Ultramafic Nodules. *Proc. Lunar Planet. Sci. Conf.10th*, 2, 2031–2050.doi:10.1016/j.oregeorev.2010.12.002

Janecky, D. R., and Seyfried, W. E., Jr (1986). Hydrothermal Serpentinization of Peridotite within the Oceanic Crust: Experimental Investigations of Mineralogy and Major Element Chemistry. *Geochimica Cosmochimica Acta* 50 (7), 1357–1378. doi:10.1016/0016-7037(86)90311-x

Jensen, L. S. (1976). *A New Cation Plot for Classifying Subalkalic Volcanic Rocks*, 66. Ministry of Natural Resources.

Jöns, N., and Schenk, V. (2007). Relics of the mozambique Ocean in the Entral Eastern African Orogen: Evidence from the Vohibory Block of Southern madagascar. *J. Metamorph. Petrology* 26, 17–28. doi:10.1111/j.1525-1314.2007.00745.x

Khedr, M. Z., and Arai, S. (2016). Chemical Variations of Mineral Inclusions in Neoproterozoic High-Cr Chromitites from Egypt: Evidence of Fluids during Chromitite Genesis. *Lithos* 240-243, 309–326. doi:10.1016/j.lithos.2015.11.029

Klemm, D., and Klemm, R. (2013). *Gold and Gold Mining in Ancient Egypt and Nubia*. Berlin: Springer, 649.

Klemm, D., Klemm, R., and Murr, A. (2001). Gold of the Pharaohs–6000 Years of Gold Mining in Egypt and Nubia. *J. Afr. Earth Sci.* 33 (3–4), 643–659. doi:10.1016/s0899-5362(01)00094-x

Klitzch, C., List, F., and Pöhlmann, A. (1987). Geological Map of Egypt (CONOCO), NG 36NE. *Qusier scale* 1, 500000.

Koutsovitis, P. (2017). High-pressure Subduction-Related Serpentinites and Metarodingites from East Thessaly (Greece): Implications for Their Metamorphic, Geochemical and Geodynamic Evolution in the Hellenic–Dinaric Ophiolite Context. *Lithos* 276, 122–145. doi:10.1016/j.lithos.2016.11.008

Kröner, A., Grieling, R., Reischmann, T., Hussein, I. M., Stern, R. J., Dürr, S., et al. (1987). Pan-African Crustal Evolution in the Nubian Segment of Northeast Africa. *Proterozoic Lithospheric Evol.* 17, 235–257. þ. doi:10.1016/0012-821X(87)90024-010.1029/gd017p0235

Kusky, T. M., and Ramadan, T. M. (2002). Structural Controls on Neoproterozoic Mineralization in the South Eastern Desert, Egypt: an Integrated Field, Landsat TM, and SIR-C/X SAR Approach. *J. Afr. Earth Sci.* 35, 107–121. doi:10.1016/s0899-5362(02)00029-5

Kyser, T. K., and Kerrich, R. (1991). "Retrograde Exchange of Hydrogen Isotopes between Hydrous Minerals and Water at Low Temperatures," in *Stable Isotope Geochemistry: A Tribute to Samual Epstein*. Editors H. P. TaylorJr, J. R. O'Neil, and I. R. Kaplan (United States: The Geochemical Society, Special Publication), 3, 409–424.

Le maitre, R. W., Bateman, P., Dudek, A., Keller, J., Lameyre, M., Le Bas, M. J., et al. (1989). "A Classification of Igneous Rocks and a Glossary of Terms," in *Recommendations of the International Union of Geological Sciences Subcommission on the Systematics of Igneous Rocks* (Oxford: Blackwell Scientific Publications), 193. https://searchworks.stanford.edu/view/1363112.

Leblanc, M. (1991). "Platinum-group Elements and Gold in Ophiolitic Complexes: Distribution and Fractionation from Mantle to Oceanic Floor," in *Ophiolite Genesis and Evolution of the Oceanic Lithosphere*. Editors T. Peters, A. Nicolas, and R. Coleman (Springer). doi:10.1007/978-94-011-3358-6_13

Li, Z. X. A., and Lee, C. T. A. (2006). Geochemical Investigation of Serpentinized Oceanic Lithospheric Mantle in the Feather River Ophiolite, California: Implications for the Recycling Rate of Water by Subduction. *Chem. Geol.* 235 (1-2), 161–185. doi:10.1016/j.chemgeo.2006.06.011

Loizenbauer, J., Wallbrecher, E., Fritz, H., Neumayr, P., Khudeir, A. A., and Kloetzli, U. (2001). Structural Geology, Single Zircon Ages and Fluid Inclusion Studies of the Meatiq Metamorphic Core Complex: Implications for Neoproterozoic Tectonics in the Eastern Desert of Egypt. *Precambrian Res.* 110 (1-4), 357–383. þ. doi:10.1016/s0301-9268(01)00176-0

McDonough, W. F., and Sun, S. S. (1995). The Composition of the Earth. *Chem. Geol.*, 120(3-4), pp. 223–253. doi:10.1016/0009-2541(94)00140-4

Mével, C. (2003). Serpentinization of Abyssal Peridotites at Mid-ocean Ridges. *Comptes Rendus Geosci.* 335, 825–852. doi:10.1016/j.crte.2003.08.006

Miyashiro, A., Shido, F., and Ewing, M. (1969). Composition and Origin of Serpentinites from the Mid-Atlantic Ridge Near 24 and 30 North Latitude. *Contr. Mineral. Pet.* 23 (2), 117–127. doi:10.1007/bf00375173

Moghadam, H. S., Khedr, M. Z., Arai, S., Stern, R. J., Ghorbani, G., Tamura, A., et al. (2015). Arc-related Harzburgite–Dunite-Chromitite Complexes in the Mantle Section of the Sabzevar Ophiolite, Iran: A Model for Formation of Podiform Chromitites. *Gondwana Res.* 27, 575–593. doi:10.1016/j.gr.2013.09.007

Nasir, S., Al-Sayigh, A. R., Al-Harthy, A., Al-Khirbash, S., Al-Jaaidi, O., Musllam, A., et al. (2007). Mineralogical and Geochemical Characterization of Listwaenite from the Semail Ophiolite, Oman. *Geochemistry* 67 (3), 213–228. doi:10.1016/j.chemer.2005.01.003

Niu, Y. (2004). Bulk-rock Major and Trace Element Compositions of Abyssal Peridotites: Implications for Mantle Melting, Melt Extraction and Post-melting Processes beneath Mid-ocean Ridges. *J. Pet.* 45 (12), 2423–2458. doi:10.1093/petrology/egh068

Noweir, A. M., Rashwan, A. A., Abu El-Ela, A. M., and El-Hashash, M. A. A. (2000). Petrology, Petrochemistry and Crustal Evolution of the Precambrian Rocks, Wadi Um Ashira, South Eastern Desert, Egypt. *Ann. Geol. Surv. Egypt* 18, Part 3, pp. 961–981. https://eurekamag.com/research/019/715/019715115.php.

O'Hanley, D. S., Kyser, T. K., and Stauffer, M. (1993). Provenance, Deformation, and Alteration History of Mafic-Ultramafic Rocks East of Amisk Lake, and the Provenance of the Mafic and Ultramafic Boundary Intrusions, in the Flin Flon Domain, Trans-Hudson Orogen. *Lithoprobe Rep.* 34, 190–206.

O'Hanley, D. S. (1996). *Serpentinites: Records of Tectonic and Petrological History*. New York and Oxford: Oxford Monographs on Geology and Geophysics, 227. doi:10.1016/0028-3932(96)00039-5

Oweiss, Kh. A., El-Naggar, A. A., Abdel Razik, K. A., Moselhy, N., and Ali, A. B. (2001). Gold Exploration at Heiani Area, South Eastern Desert, Egypt. *Ann. Geol. Surv. Egypt* 24, 435–450.

Palandri, J. L., and Reed, M. H. (2004). Geochemical Models of Metasomatism in Ultramafic Systems: Serpentinization, Rodingitization, and Sea Floor Carbonate Chimney Precipitation. *Geochimica Cosmochimica Acta* 68 (5), 1115–1133. doi:10.1016/j.gca.2003.08.006

Parkinson, I. J., and Pearce, J. A. (1998). Peridotites from the Izu–Bonin-Mariana Forearc (ODP Leg 125): Evidence for Mantle Melting and Melt-Mantle Interaction in a Supra-subduction Zone Setting. *J. Petrology* 39, 1577–1618. doi:10.1093/petroj/39.9.1577

Paulick, H., Bach, W., Godard, M., De Hoog, J. C. M., Suhr, G., and Harvey, J. (2006). Geochemistry of Abyssal Peridotites (Mid-Atlantic Ridge, 15°20′N, ODP Leg 209): Implications for Fluid/rock Interaction in Slow Spreading Environments. *Chem. Geol.* Volume 234, Issues 3–4, 179–210. doi:10.1016/j.chemgeo.2006.04.011

Pearce, J. A., Barker, P. F., Edwards, S. J., Parkinson, I. J., and Leat, P. T. (2000). Geochemistry and Tectonic Significance of Peridotites from the South Sandwich Arc-Basin System, South Atlantic. *Contributions Mineralogy Petrology* 139, 36–53. doi:10.1007/s004100050572

Pearce, J. A. (2008). Geochemical Fingerprinting of Oceanic Basalts with Applications to Ophiolite Classification and the Search for Archean Oceanic Crust. *Lithos* 100, 14–48. doi:10.1016/j.lithos.2007.06.016

Pearce, J. A., Lippard, S. J., and Roberts, S. (1984). "Characteristics and Tectonic Significance of Supra-subduction Zone Ophiolites," in *Geological Society, London, Special Publications*. Editors B. P. Kokelaar and M. F. Howells (University of Colorado Boulder) 16, 77–94. doi:10.1144/gsl.sp.1984.016.01.06

Pfeifer, H. R. (1990). *Major and Trace Element Discrimination Diagrams to Determine Possible Protoliths of Orogenic Ultramafic Rocks*. Universite de Lausanne. http://in.bgu.ac.il/teva/geological/eng/ykatzir/Documents/1999%20Katzir%20et%20al%20JMG.pdf.

Pirajno, F. (2009). "Hydrothermal Processes and Wall Rock Alteration," in *Hydrothermal Processes and Mineral Systems* (Dordrecht: Springer), 73–164. doi:10.1007/978-1-4020-8613-7_2

Polat, A., and Hofmann, A. W. (2003). Alteration and Geochemical Patterns in the 3.7–3.8 Ga Isua Greenstone Belt, West Greenland. *Precambrian Res.* 126 (3-4), 197–218. doi:10.1016/S0301-9268(03)00095-0

Ries, A., Shackelton, R., Graham, R., and Fitches, W. (1983). Pan-African Structures, Ophiolites and Mélange in the Eastem Desert of Egypt: a Traverse at 26°N. *J. Geol. Soc.* 140, 75–95. doi:10.1144/gsjgs.140.1.0075

Salters, V. J. M., and Stracke, A. (2004). Composition of the Depleted Mantle. *Geo-chem Geophys Geosys* 5, Q05B07. doi:10.1029/2003gc000597

Seyfried, W. E., and Dibble, W. E. (1980). Seawater - Peridotite Interaction at 300°C and 500 Bars: Implications for the Origin of Oceanic Serpentinites. *Geochimica Cosmochimica Acta* 44, 309–321. doi:10.1016/0016-7037(80)90139-8

Shackleton, R. M. (1994). Review of Late Proterozoic Sutures, Ophiolitic Mélanges and Tectonics of Eastern Egypt and North-East Sudan. *Geol. Rundsch* 83 (3), 537–546. þ. doi:10.1007/bf01083226

Shackleton, R. M., Ries, A. C., Graham, R. H., and Fitches, W. R. (1980). Late Precambrian Ophiolitic Mélange in the Eastern Desert of Egypt. *Nature* 285, 472–474. doi:10.1038/285472a0

Shaheen, T. M. (2012). *Geology, Geochemistry and Petrotectonic of the Basement Rocks at Gabal El Dob Area, North Eastern Desert, Egypt*. Al-Azhar University, PhD Thesis, 349p.

Snow, J. E., and Dick, H. J. B. (1995). Pervasive Magnesium Loss by Marine Weathering of Peridotite. *Geochimica Cosmochimica Acta* 59 (20), 4219–4235. doi:10.1016/0016-7037(95)00239-V

Soliman, N. M., El-Desoky, H. M., Heikal, M. A., and Abdel-Rahman, A. M. (2021). Using ASTER Images and Field Work Data for Geological Mapping Around Wadi Umm Ashira and Wadi Tilal Al-Qulieb, Northwestern Part of Wadi Allaqi, South Eastern Desert, Egypt. *Arabian J. Geosciences* 14 (18), 1–19. doi:10.1007/s12517-021-08234-5

Stern, R. J. (1994). Arc Assembly and Continental Collision in the Neoproterozoic East African Orogen: Implications for the Consolidation of Gondwanaland. *Annu. Rev. Earth Planet. Sci.* 22, 319–351. doi:10.1146/annurev.ea.22.050194.001535

Stern, R. J., Johnson, P. R., Kröner, A., and Yibas, B. (2004). Neoproterozoic Ophiolites of the Arabian-Nubian Shield. *Dev. Precambrian Geol.* 13, 95–128. doi:10.1016/s0166-2635(04)13003-x

Stouraiti, C., Pantziris, I., Vasilatos, C., Kanellopoulos, C., Mitropoulos, P., Pomonis, P., et al. (2017). Ophiolitic Remnants from the Upper and Intermediate Structural Unit of the Attic-Cycladic Crystalline Belt (Aegean, Greece): Fingerprinting Geochemical Affinities of Magmatic Precursors. *Geosciences* 7 (1), 14. doi:10.3390/geosciences7010014

Sultan, M., Arvidson, R. E., Sturchio, N. C., and Guinness, E. A. (1987). Lithologic Mapping in Arid Regions with Landsat Thematic Mapper Data: Meatiq Dome, Egypt. *Geol. Soc. Am. Bull.* 99, 748–762. doi:10.1130/0016-7606(1987)99<748:lmiarw>2.0.co;2

Sun, S.-S., and McDonough, W. F. (1989). Chemical and Isotopic Systematics of Oceanic Basalts: Implications for Mantle Composition and Processes. *Geol. Soc. Spec. Publ.* 42, 313–345. doi:10.1144/GSL.SP.1989.042.01.19

Surour, A. A. (2017). Chemistry of Serpentine "Polymorphs" in the Pan-African Serpentinites from the Eastern Desert of Egypt, with an Emphasis on the Effect of Superimposed Thermal Metamorphism. *Min. Pet.* 111, 99–119. doi:10.1007/s00710-016-0460-4

Tahir, M., Imai, A., Takahashi, R., and Yano, S. (2018). Ore Genesis and Geochemical Characteristics of Carbonate-Hosted Talc Deposits in Nangarhar Province, Afghanistan. *Resour. Geol.* 68 (4), 352–372. þ. doi:10.1111/rge.12174

Takla, M. A. (1982). "Chromites from the Bergen Arcs Ultramafics," in *Neues Jahrbuch für Mineralogie - Abhandlungen*. Southern Norway: Schweizerbart science publishers, 144, 56–72. Band 144 Heft 1. doi:10.1127/njma/144/1982/56

Takla, M. A., Noweir, A. M., and Aly, S. A. (1975). Ore Mineralogy of the Serpentinites of Bir El-Kubbaniya Um Khors Area. *Egypt Chem. Erde* 34, 244–250.

Ucurum, A., and Larson, L. T. (1999). Geology, Base-Precious Metal Concentration and Genesis of the Silica-Carbonate Alteration (Listwaenites) from Late Cretaceous Ophiolitic Mélanges at Central East Turkey.þ *Chem. Der Erde-Geochemistry*, vol.59, no.2, pp.77–104, https://hdl.handle.net/20.500.12418/11747.

Ucurum, A., Larson, L. T., and Boztug, D. (1996). Geology, Geochemistry, and Petrology of the Alkaline Subvolcanic Trachyte-Hosted Iron Deposit in the Karakuz Area, Northwestern Hekimhan-Malatya, Turkey. *Intern. Geol. Rev.*, 38(11), 995–1005.

Ucurum, A. (2000). Listwaenites in Turkey: Perspectives on Formation and Precious Metal Concentration with Reference to Occurrences in East-Central Anatolia. *Ofioliti* 25 (1), 15–29. doi:10.4454/OFIOLITI.V25I1.110

Walker, K. R., Joplin, G. A., Lovering, J. F., and Green, R. (1960). Metamorphic and Metasomatic Convergence of Basic Igneous Rocks and Limemagnesia Sediments of the Precambrian of North-Western Queensland. *Jour. Geol. Soc. Aust.* 6, 149–178. doi:10.1080/00167615908728504

Wenner, D. B., and Taylor, H. P., Jr (1974). D/H and O18/O16 Studies of Serpentinization of Ultramaflc Rocks. *Geochimica Cosmochimica Acta* 38 (8), 1255–1286. doi:10.1016/0016-7037(74)90120-3

Whattam, S. A., and Stern, R. J. (2011). The 'subduction Initiation Rule': a Key for Linking Ophiolites, Intra-oceanic Forearcs, and Subduction Initiation. *Contrib. Mineral. Pet.* 162, 1031–1045. doi:10.1007/s00410-011-0638-z

Workman, R. K., and Hart, S. R. (2005). Major and Trace Element Composition of the Depleted MORB Mantle (DMM). *Earth Planet. Sci. Lett.* 231 (1-2), 53–72. doi:10.1016/j.epsl.2004.12.005

Zakaly, H. M., Uosif, M. A., Uosif, M. A., Madkour, H., Tammam, M., Issa, S., et al. (2019). Assessment of Natural Radionuclides and Heavy Metal Concentrations in Marine Sediments in View of Tourism Activities in Hurghada City, Northern Red Sea, Egypt. *J. Phys. Sci.* 30, 21–47. doi:10.21315/jps2019.30.3.3

Zimmer, M., Kröner, A., Jochum, K. P., Reischmann, T., and Todt, W. (1995). The Gabal Gerf Complex: A Precambrian N-MORB Ophiolite in the Nubian Shield, NE Africa. *Chem. Geol.*, 123 (1–4), 29–51. doi:10.1016/0009-2541(95)00018-H

Zindler, A., and Hart, S. (1986). Chemical Geodynamics. *Annu. Rev. Earth Planet. Sci.* 14 (1), 493–571. doi:10.1146/annurev.ea.14.050186.002425

Zoheir, B., and Klemm, D. (2007). The Tectono-Metamorphic Evolution of the Central Part of the Neoproterozoic Allaqi-Heiani Suture, South Eastern Desert of Egypt. *Gondwana Res.* 12, 289–304. doi:10.1016/j.gr.2006.10.005

Zoheir, B., and Lehmann, B. (2011). Listvenite-lode Association at the Barramiya Gold Mine, Eastern Desert, Egypt. *Ore Geol. Rev.*, 39(1-2), 101–115.doi:10.1016/j.oregeorev.2010.12.002

Conflict of Interest: The authors declare that the research was conducted in the absence of any commercial or financial relationships that could be construed as a potential conflict of interest.

The reviewer MA declared a shared affiliation with the author BNAS to the handling editor at the time of review.

Publisher's Note: All claims expressed in this article are solely those of the authors and do not necessarily represent those of their affiliated organizations, or those of the publisher, the editors, and the reviewers. Any product that may be evaluated in this article, or claim that may be made by its manufacturer, is not guaranteed or endorsed by the publisher.